USING SELF-ORGANIZING MAPS TO DETAIL SYNOPTIC CONNECTIONS BETWEEN CLIMATE INDICES AND ALASKA WEATHER

By

Reynir Winnan

RECOMMENDED:

Dr. Renate A. Wackerbauer

Dr. John E. Walsh

Dr. Richard L. Collins

Dr. Uma S. Bhatt
Advisory Committee Chair

Dr. Uma S. Bhatt
Chair, Department of Atmospheric Sciences

APPROVED:

Dr. Paul W. Layer
Dean, College of Natural Science and Mathematics

Dr. John C. Eichelberger
Dean of the Graduate School

7 December 2015
Date

USING SELF-ORGANIZING MAPS TO DETAIL SYNOPTIC CONNECTIONS BETWEEN CLIMATE INDICES AND ALASKA WEATHER

A

Thesis

Presented to the Faculty

of the University of Alaska Fairbanks

in Partial Fulfillment of the Requirements

for the Degree of

MASTER OF SCIENCE

By

Reynir C. Winnan, B.S.

Fairbanks, Alaska

December 2015

Abstract

Seasonal forecasts for Alaska strongly depend on the phases of Pacific Decadal Oscillation (PDO), El Niño-Southern Oscillation (ENSO), and warm water in the North Pacific called the North Pacific Mode or more popularly the "Pacific blob." The canonical descriptions of these climate indices are based on seasonal averages, and anomalies that are based on a long-term mean. The patterns highlight general geographical placement and display a sharp contrast between opposing phases, but this may be misleading since seasonal averages hide much of the synoptic variability. Self-organizing maps (SOMs) are a way of grouping daily sea level pressure (SLP) patterns, over many time realizations into a specified set of maps (e.g. 35 maps) that describe commonly occurring patterns. This study uses the SOMs in the context of climate indices to describe the range of synoptic patterns that are relevant for Alaska. This study found that the patterns common during a given phase of the PDO include subtle differences that would result in Alaska weather that is very different from what is expected from the canonical PDO description, thus providing some explanation for recent studies that find the PDO link to Alaska climate is weakening. SOMs analysis is consistent with recent studies suggesting that the pattern responsible for the 2014 Pacific warm blob is linked to tropical sea-surface temperature (SST) forcing. An analysis of the summer SLP SOMs in the context of Alaska wildland fires was also conducted. This analysis identified several commonly occurring patterns during summers with large areas burned. These patterns are characterized by low pressure in the Bering Sea, which would be consistent with increased storm activity and thus an ignition source for the fires. Identifying synoptic patterns that occur during a particular phase of a teleconnection index contributes towards understanding the mechanisms of how these indices influence the weather and climate of Alaska.

Table of Contents

Page

List of Figures

Page

Page

Page

List of Tables

Page

Acknowledgments

I would like to thank my advisor, Uma Bhatt, for her instruction, guidance, enthusiasm, and enormous amounts of time put toward the process of completing this project. I would also like to thank the members of my committee, John Walsh, Rich Collins, and Renate Wackerbauer for their suggestions, support, and expert advice. Thank you to Rick Thoman for sharing his wealth of meteorological knowledge, and for helping to target practical objectives with the tools and concepts in this project with the additional support of the National Weather Service and Alaska Fire Science Consortium. Thank you to Elizabeth and John Cassano for being fantastic resources for all SOM information. Thank you to Barbara Day for tireless administrative support. This work was supported through funding by the Department of Energy through grant number DE-SC0001898 and through a teaching assistantship from the College of Natural Science and Mathematics at UAF. Finally, thank you to my family, classmates and friends both inside and outside UAF for welcome distractions, tolerance of long conversations, interesting—if not entirely appropriate—suggestions for titles and other language in this manuscript, inspiration, and for generally making life better while this project was completed.

Chapter 1 – Introduction

1.1 – Seasonal forecasting in Alaska

Forecasting weather and climate in Alaska is not for the faint of heart, for the same reason most things in Alaska are not for the faint of heart. Limited resources are available to address a climate characterized by harsh and highly varied conditions, where the Interior Alaska city of Fairbanks swings from a wintertime average minimum temperature of -11.6 degrees F to a summertime average maximum temperature of 64.3 degrees F. Wintertime average precipitation increases from 2.90 inches in the Northeast Interior to 70.37 inches in the Northeast Gulf (Shulski and Wendler 2007; National Climatic Data Center 2015). Alaska has 13 official climate divisions (Bieniek et al. 2012), monitored by a network of 173 weather stations and observation sites (National Weather Service 2015) that, together, cover a complex topography, and a surface area one-fifth the size of the contiguous United States, spanning 20 degrees of latitude and 50 degrees of longitude in the North Pacific (Figure 1.1).

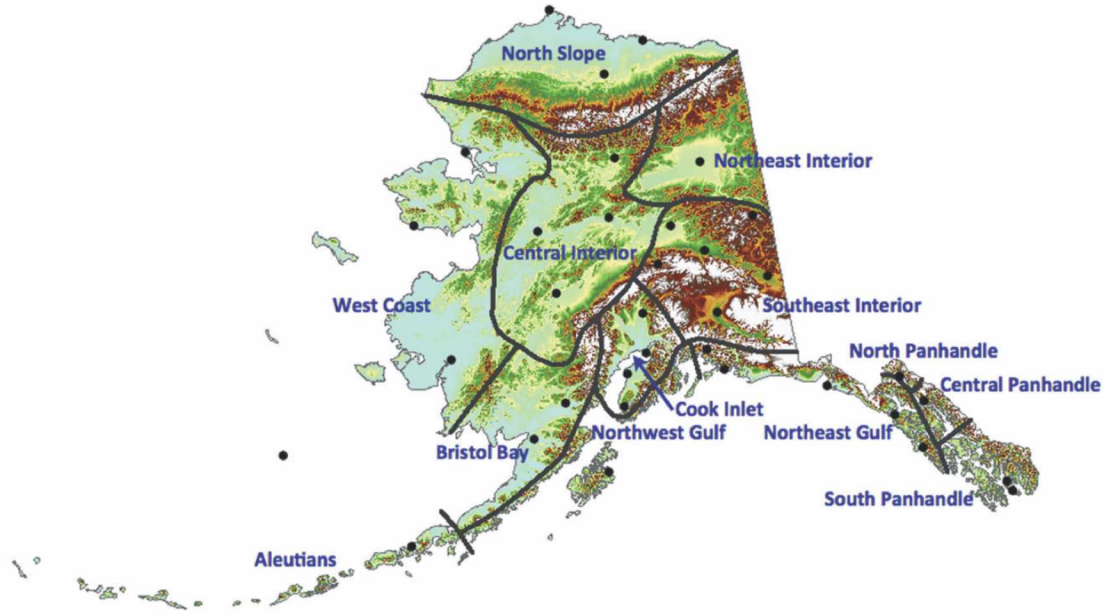

Figure 1.1 Alaska's thirteen climate divisions group regions with similar climate variability. From Bieniek et al. (2012).

In comparison, Texas, the second largest state in the US, has 166 weather stations and observation sites (National Weather Service 2015), and is 60% smaller than Alaska. Alaska residents rely heavily on seasonal forecasts that are produced with heavy influence from large-scale climate indices, like El Niño-Southern Oscillation (ENSO), and the Pacific Decadal Oscillation (PDO) (Barnston and He 1996; Mantua et al. 1997; Bieniek et al. 2011). This influence simplifies forecasting, but can yield misleading results, particularly if the relationship between the indices and Alaskan climate weakens or has subtle dependencies on the details of the patterns represented by the indices (McAfee 2014). Examining these indices in finer detail may show subtle features with a more robust relationship with Alaskan seasonal climate.

Alaska's high latitude and proximity to the Pacific Ocean positions the state within the influence of a number of large-scale climate circulations, some of which are changing in regard to their relationship with Alaska weather. The two climate oscillations given the most focus in this thesis are the PDO and ENSO, since some of the most pronounced features and effects of these circulations influence Alaska (McAfee 2014). While the time scale for the PDO is 20-30 years, the timescale of ENSO is 2-8 years (Figure1.2). The connection PDO and ENSO have with each other (Newman et al. 2003), and the results of their competing phases complicate their correlation with Alaskan climate variability. Another index, referred to as the North Pacific Warm Blob is characterized by anomalously warm ocean temperature anomalies in the Northeast Pacific associated with anomalous high pressure in the region during winter (Bond et al. 2015). Yet another pattern of variability is the Arctic Oscillation (AO), which is defined as the difference in atmospheric pressure between the polar regions and the mid-latitudes. The positive phase is characterized by a stronger latitudinal pressure gradient due to anomalously low pressure in the polar region, and anomalously high pressure over the mid-latitudes (Thompson and Wallace 1998). Each has a particular effect on Alaska, but the net pressure and circulation anomalies may be enhanced or diminished depending on the phase (positive, negative, neutral) of each index (Bond and Harrison 2006). This study will focus on the winter effects of the PDO, with and without the influence of

ENSO. In addition, this study examines the winter and summer effects of the Pacific blob and summer patterns related to forest fires in Alaska.

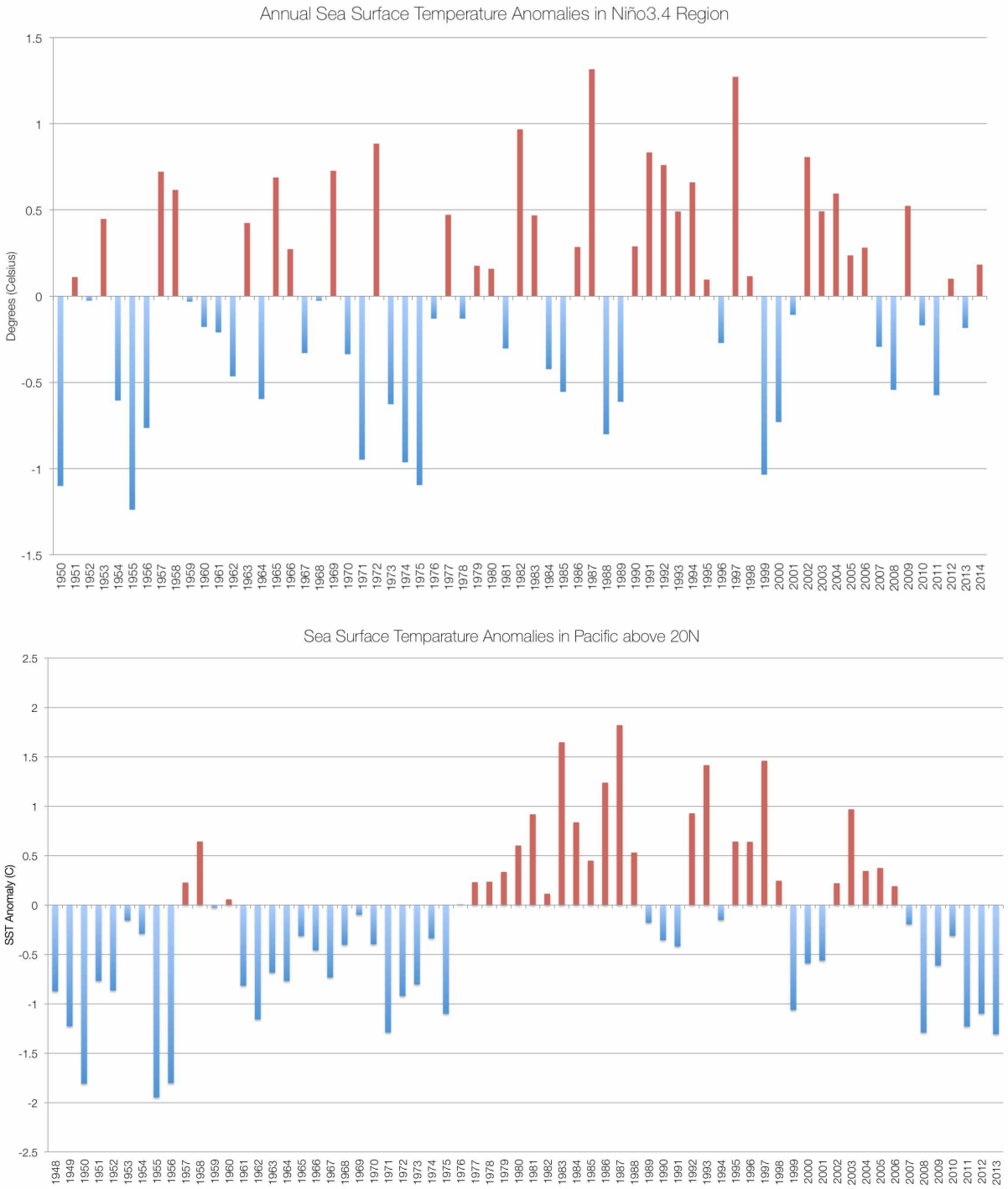

Figure 1.2 top: ENSO time series, defined by SST anomalies in Niño3.4 region. bottom: PDO time series, defined by SST anomalies above 20N in Pacific.

1.2 – Pacific Decadal Oscillation (PDO)

The PDO is the principal component (PC) of the first empirical orthogonal function (EOF) of detrended sea surface temperature (SST) in the North Pacific (Mantua et al. 1997). More specifically, the pattern that describes most of the variability in the North Pacific SST has warm and cold SST anomalies in the North Pacific. This pattern describes two phases that fluctuate over a period of 20-30 years (Figure 1.2). The positive (warm) PDO phase is characterized by the anomalously cool SSTs in the central North Pacific, and warm SSTs in the Equatorial and northeastern Pacific, with just the opposite during the negative (cool) PDO phase (Figure 1.3).

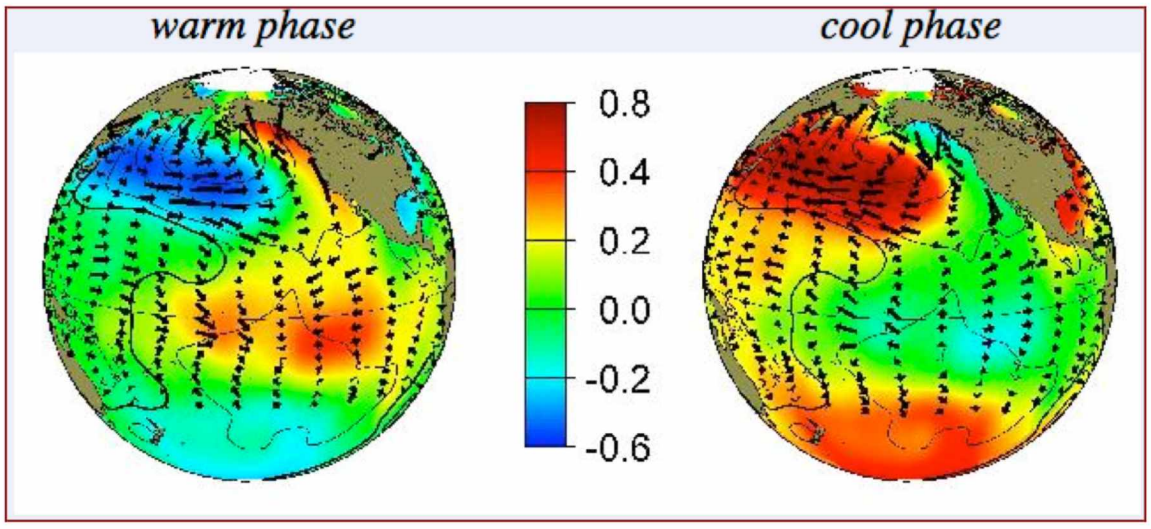

Figure 1.3 Warm and cool phases of the Pacific Decadal Oscillation (PDO). Colored shading represents SST anomalies in degrees Celsius. Vectors represent anomalous wind direction. From Mantua (2000).

The positive PDO phase SST pattern is correlated with warmer-than-normal temperatures in Alaska during the cold season, and is characterized by a strong eastward shifted wintertime Aleutian Low (Trenberth 1990; Papineau 2001). The negative phase displays the opposite pattern. This correlation also appears to be stronger in winter than in the summer, based on analysis up to the year 2000 (Papineau 2001).

Since the PDO and ENSO are both associated with SST anomalies in the mid-latitude and Equatorial Pacific, both signals are present in North Pacific patterns (Newman et al. 2003; Mills and Walsh 2013). In order to remove the influence of ENSO from the PDO signal, a residual PDO (rPDO) was constructed. To produce the rPDO, a linear regression between the PDO and the Bivariate ENSO Time Series (BEST) index (Smith and Sardeshmukh 2000) is used to predict the ENSO index, which is then subtracted from the observed PDO index. The extended winter rPDO (Eq 1.1) in a given year (t) is the PDO in same year (PDO(t)) minus the November-March ENSO index (ENSO(t-1)) of the previous year (t-1). Note that a 5-month running mean has been applied to the ENSO index. This methodology is from McAfee (2014), which was based on concepts from Mills and Walsh (2013).

$$rPDO(t) = PDO(t) - 0.75ENSO(t-1) + 0.05 \qquad \text{Eq. 1.1}$$

The correlation between the PDO and Alaska climate appears to be breaking down. The last negative phase included enough anomalous warming of the Bering Sea and North Pacific to erode the significant difference between positive and negative phases. This breakdown is attributed to instability in the relationship between the PDO and Alaska temperatures, the influence of climate change and other climate variability on the PDO, or a consequence of a small sample size in the observational record of PDO phases (McAfee 2014). Maps of the correlation and regression of the PDO on surface air temperature (SAT) show a weaker correlation, and a slight shift in geographical placement since 1976 (Figure 1.4). Bourne et al. (2010) found that the correlation between the PDO and SAT and Alaska weather stations (Fairbanks, Kotzebue, Bethel, Anchorage, King Salmon, and McGrath) notably weakened after 1989. Curiously, the correlation remained unchanged (~0.30) between the PDO and SAT in Barrow.

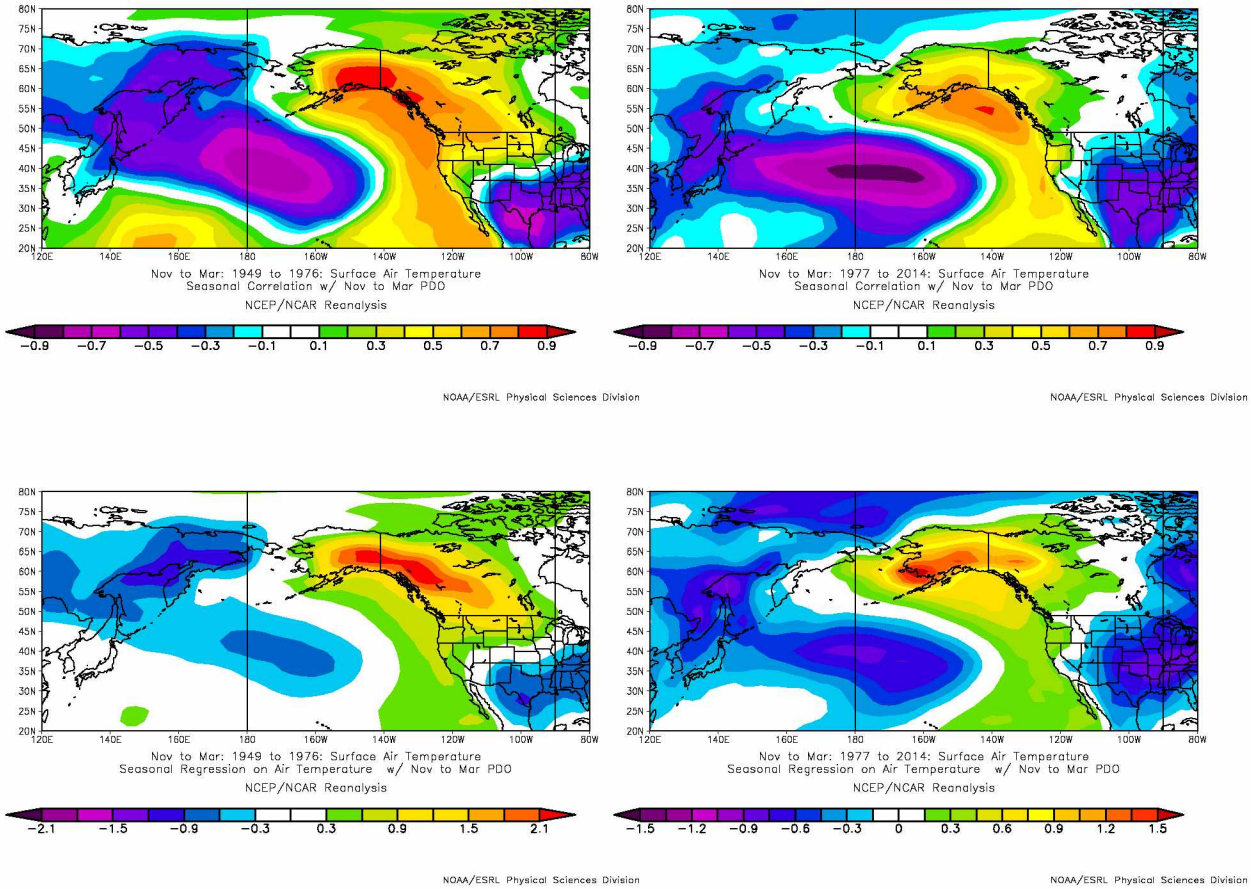

Figure 1.4 Surface air temperature seasonal correlation (top plots) and seasonal regression (bottom plots; units in degrees C) with November – March PDO index for 1949 – 1976 (left) and for 1977 – 2014 (right). Images provided by the NOAA/ESRL Physical Sciences Division, Boulder Colorado from their Web site at http://www.esrl.noaa.gov/psd/; retrieved July 2015.

1.3 – North Pacific Warm Blob

Beginning in October 2013, and continuing until January 2014, anomalous high SLP was observed over the eastern North Pacific. With peak anomalies around 10 hPa, this high pressure was a record for the time period 1949-2014. This high pressure suppressed wind in the region, weakening wind-forced currents, wind-generated mixing, and surface heat loss. The result was an area of extremely warm SST—greater than 2.5 degrees C at its peak in February 2014—in the south central Gulf of Alaska, and the region 55N-45N and 150W-130W (Figure 1.5).

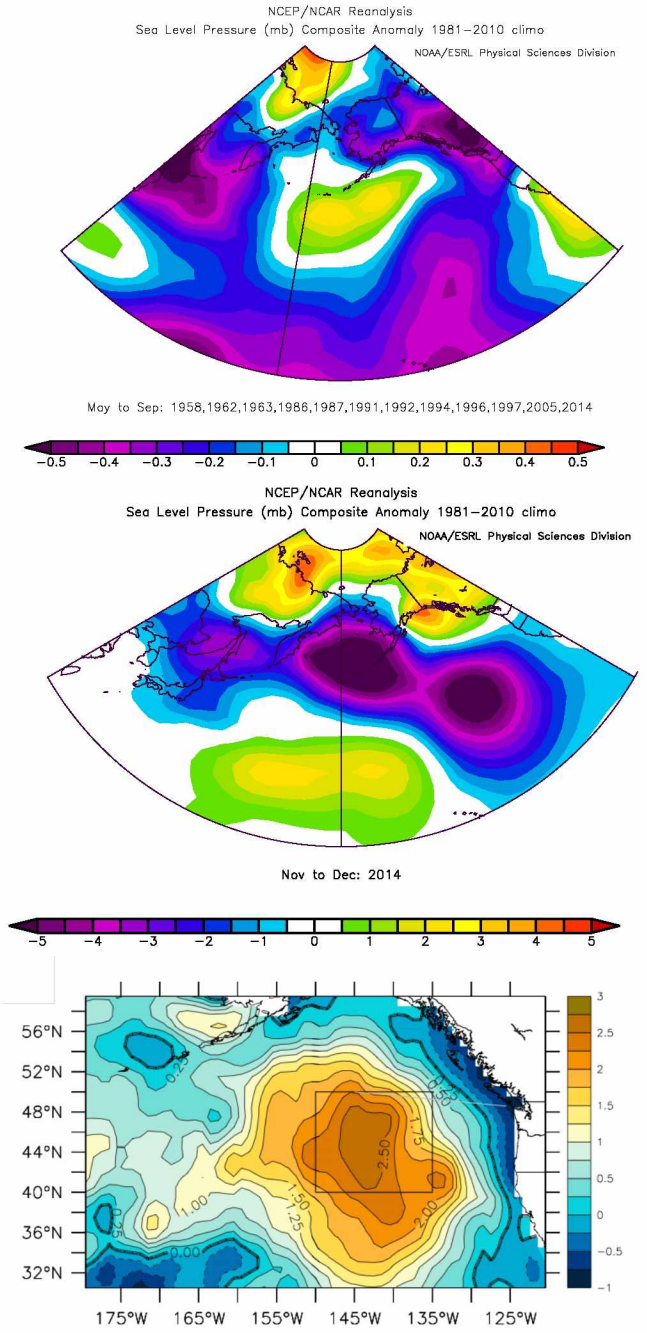

Figure 1.5 Top plot is the mean SLP pattern for NDJFM 2014. Middle plot is the SLP anomaly for NDJFM 2014. Images provided by the NOAA/ESRL Physical Sciences Division, Boulder Colorado from their Web site at http://www.esrl.noaa.gov/psd/; retrieved July 2015. Bottom plot is the SST anomalies in degrees Celsius in the North Pacific for February 2014 (From Bond et al. 2015).

The anomalous SST moved towards the Pacific Northwest coast by the spring of 2014, and persisted for another year into the spring of 2015 and beyond. The expansive area of warm SST has come to be termed 'the Blob' (Bond et al. 2015). Pop culture has embraced the term 'blob' for obvious reasons, but for clarity and precision—particularly when discussing the opposite conditions of the warm blob—this paper will refer to the phenomenon as the positive (warm) and negative (cold) phases of the North Pacific Mode (NPM) (Hartmann 2015). In the discussion of phases of this phenomenon, an SST anomaly greater than, or equal to, one standard deviation (0.5) above the mean SST anomaly (0.0) in the region will be referred to as positive NPM, while negative NPM will refer to the opposite case (Figure 1.6). The winter SLP anomalies associated with the Pacific positive phase of the NPM can be characterized by a persistent high-pressure area over the eastern Gulf of Alaska and is considered to have forced the SST anomaly signature of the Pacific positive NPM (Figure 1.7a). Anomalously high SLP in winter is associated with weak atmospheric near-surface flow and reduced turbulent heat (sensible and latent) loss from the ocean to the atmosphere, consistent with a mid-latitude atmospherically forced SST anomaly. The same map for the negative NPM shows no particular anomaly in the region, as the high pressure is located further west, over the Aleutian Islands (Figure 1.7b).

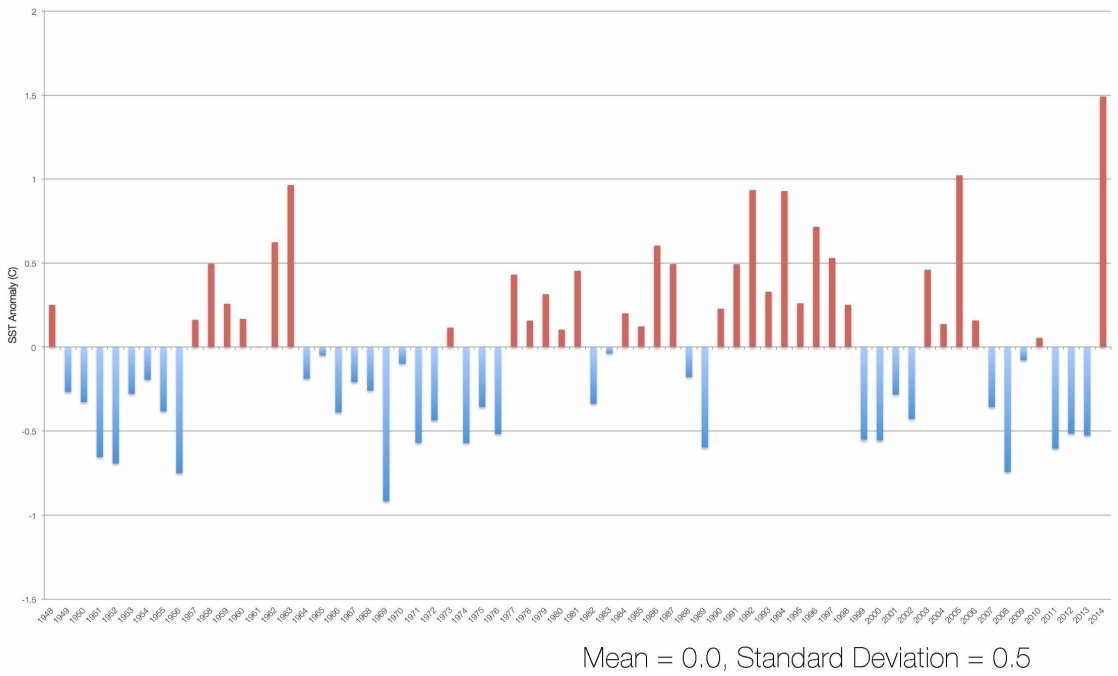

Figure 1.6 Time series of SST anomaly in the eastern North Pacific (55N-45N and 150W-130W) over the region of largest SST patterns associated with the North Pacific mode (Hartmann 2015).

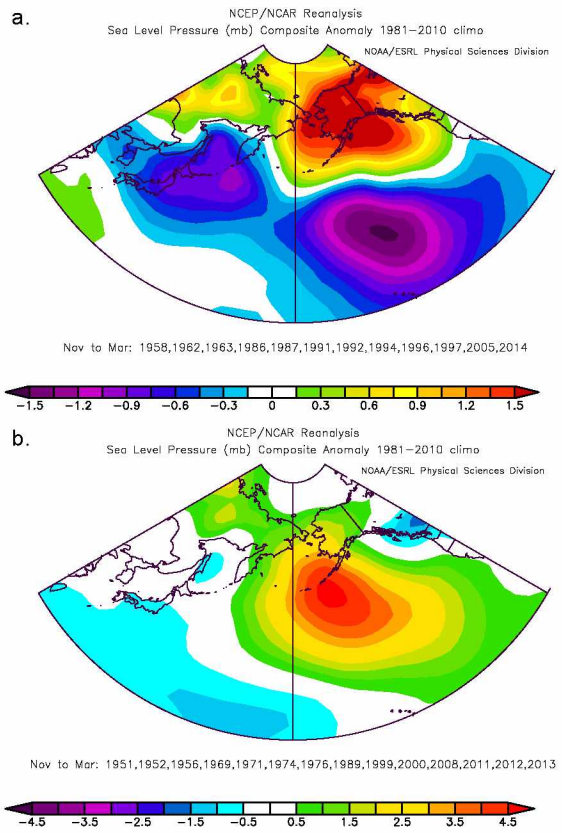

Figure 1.7 a) Sea level pressure composite anomaly for winter years with a positive NPM (see Table 2.1), b) Sea level pressure composite anomaly for winter years with a negative NPM. Data for this plot are from NOAA/ESRL, Boulder, CO, at http://www.esrl.noaa.gov/psd/; retrieved July 2015.

The presence of the positive NPM during late 2013 to spring 2015 coincides with record warm surface air temperatures (SAT) in the Pacific Northwest during the same period. A mild correlation (0.42) between February SST in the NPM region and the following March-May SAT in Washington state for the period 1949-2014 suggests a potential predictive relationship between SST in the region and SAT in the Pacific Northwest. However, no such linear correlation exists between NPM region SST and precipitation in the Pacific Northwest (Bond et al. 2015).

The mechanism that produces the NPM has not been completely established, but it is generally thought that the NPM is linked to tropical SST forcing. Seager et al. (2015) and Hartmann (2015) propose that there is a teleconnection between warm SST anomalies in the western tropical Pacific and the anomalous high pressure in the eastern Gulf of Alaska. The high pressure resulted in a warm SST anomaly in the North Pacific, which also served to strengthen the persistence of the anomalous high pressure. This pattern is thought to be a prominent driver of the record warm winter of the Pacific Northwest, and a contributor to the current drought in California (Seager et al. 2015).

1.4 – Canonical weakening

The indices discussed in this thesis are typically quantified in terms of temperature or pressure anomalies. However, the general atmospheric patterns ascribed to these circulations are constructed from averages of many synoptic patterns within a large area, where the most prevalent patterns tend to define the circulation (Xue et al. 2003). For example, a time series of the average Sea Level Pressure (SLP) over the North Pacific shows a lower than normal SLP during the November-March cold season between 1977 and 1986, suggesting a strengthened Aleutian Low following a shift to a positive PDO phase. This was consistent with patterns of thermal advection that would produce observed warm temperature anomalies over Alaska, and cool temperature anomalies in the central and western North Pacific (Trenberth 1990).

Averages can be useful for the overall picture, but they can also omit important details. Depending on the forecast purpose, it may be important to more precisely describe the most common types of synoptic patterns that comprise the Aleutian Low during a positive or negative phase of the PDO. This finer granularity will better describe the center of the Aleutian Low in sufficient detail so that persistent patterns can be identified and exploited for prediction. The detailed breakdown into multiple patterns helps to identify the preferred location of the low and better describes the surrounding pressure

pattern. The seasonal average pattern is not able to convey the set of synoptic patterns that prevail during any given phase of a large-scale climate index.

Climate indices are generally classified into distinct positive and negative phases, with the changes between them described as “reversals in the prevailing polarity” (Mantua et al. 1997). The positive and negative are so named because they are quantified by positive and negative anomalies from a long-term normal (Figure 1.8).

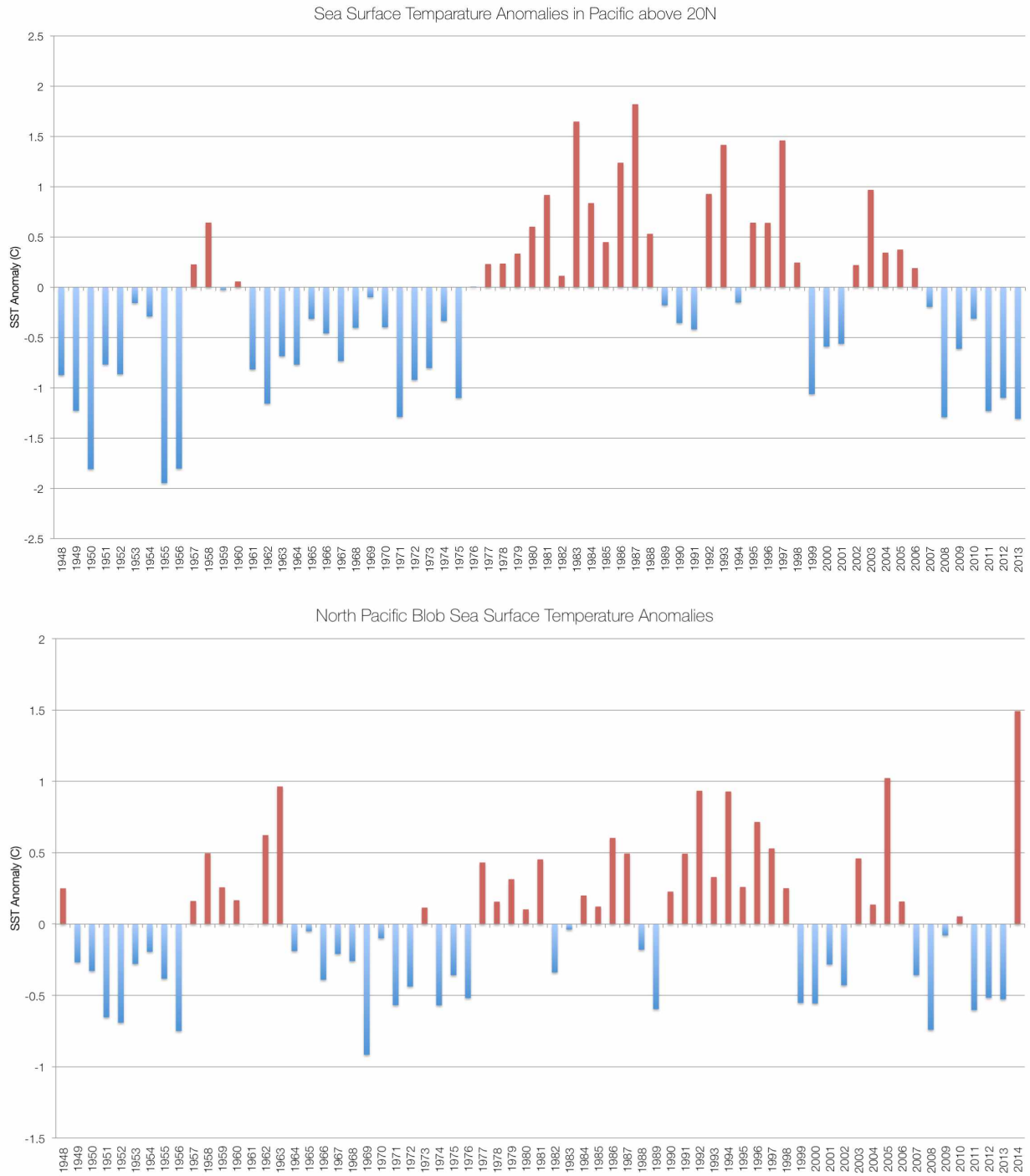

Figure 1.8 Top plot: Standardized values of PDO index, derived as leading PC of monthly SST anomalies poleward of 20N in the North Pacific for 1948-2013
Bottom plot: 1948-2014 Data for the NPM subset was NOAA ERSST V3 data provided by NOAA/OAR/ESRL PSD, from their website at http://www.esrl.noaa.gov.psd/; retrieved July 2015. Domain used is 55N-45N and 150W-130W, from Bond et al. 2015.

However, this type of polarity is not necessarily applied to the synoptic patterns that characterize each phase. A change in phase may instead suggest that a different synoptic pattern becomes more likely, rather than a complete switch to polar-opposite conditions. The correlations between a given climate pattern and regional climate that determine these climate indices may also be flawed due to small datasets, or incomplete capturing of the physical properties connecting the pattern and the climate (McAfee 2014).

1.5 – Alaska fire weather

A major feature related to Alaska summer climate is statewide wildland fires. The conditions that favor wildfires, are dry periods followed by a short period of storms that produce lightning strikes. Some evidence suggests the influence of ENSO, since conditions favored by the phases of ENSO are similar to conditions favored by big or small fire years, and 15 out of the 17 biggest Alaska fire years occurred during strong or moderate El Niño years (Hess et al. 2001). Further, 8 out of the 10 biggest fire years used in this study occurred during strong or moderate El Niño years. The potential connection to the strong ENSO signal, and a substantial change in the SLP anomaly pattern between big and small fire years suggests some element of predictability. To take advantage of any predictability will require identifying synoptic patterns favored by each year that produce the fire-favorable conditions, and the likely sequence with which they occur. This study found that patterns favored by years with a lot of fire activity prominently feature an area of low pressure and southerly flow into Alaska, while patterns favored by years with low fire activity, featured more high pressure.

Variations in spatial temperature and pressure anomalies that define the relationships central to these indices confuse an already complex process, and suggest the need for new sources of predictability, with additional forecast tools and strategies. Often, predictability comes from correlation between a climate index's associated anomalies for variables like SST with the temperature or precipitation profiles in a region of

interest, during a particular season. If such a correlation weakens, the predictability is lost.

Analyzing the variety of synoptic patterns that occur under the phases of each climate index give a more direct physical explanation of the effect of a particular phase and regional climate, and may better capture the non-linear aspects of the relationship. For example, taking advantage of the SOM's continuous distribution of synoptic maps, this study shows that in some cases, the polarity between phases of a given index is not a result of favorability for opposite conditions, but rather strong prevalence of a given pattern in one phase, and weak or no occurrence of the same pattern in the opposite phase. This is a subtle, but important distinction that may better define complicated indices, and is displayed very well by self-organizing maps. In this study, a series of Self-Organizing Maps (SOMs) is constructed to catalogue the variety of synoptic patterns present in the Pacific during the different phases of PDO, ENSO, NPM, and fire years. These maps will be stratified based on the phase of a given index in an attempt to explain the nature of the connections between PDO and recent Alaska seasonal climate, and the potential predictive ability of the NPM region for wildfires during Alaskan summers.

Chapter 2 – Methods

2.1 – Self-organizing maps

2.1.1 - Review of SOMs: how they work and advantages

Self Organizing Maps (SOMs) use an algorithm for unsupervised learning to establish a user-specified number of "nodes" that represent a model of some observed multidimensional data. A "node" in climate science can be thought of as a synoptic map of sea level pressure or some other physical variable. The user specifies the number nodes or maps then initializes each node with a random set of data. The set of observed maps are compared to each "node" and a "best match" is determined. The "best match" node and some of the surrounding nodes are then adjusted to more closely represent the observed map. All of the observed maps are compared to the nodes in this manner and the nodes are adjusted. The process concludes when the collection of nodes converge to an array of "nodes" or maps, which can be thought of as the most typical patterns within the input data (Kohonen 1990; Hewitson and Crane 2002). This method can extract the most common synoptic weather patterns from many decades of daily SLP maps and compress the information into a set of the most commonly occurring patterns.

The first step in producing a SOM is initializing the weights of the reference vectors for each node. Each reference vector is the same dimension as an input record. In this study, the input variable is a time series of SLP on a 17 X 33 (latitude-by-longitude) grid, so the reference vector would be the map size established by multiplying number of latitudinal points and longitudinal points (561). The weight for the initialized reference vectors is generally first set as a random value. In this study, the nodes were initialized with randomly selected daily SLP fields. The final results were not sensitive to the choice of the SLP map for initialization.

In order to find the node that best matches an input record, each input record is compared to each reference vector, and the program computes the Euclidean distance

as a metric for similarity between a node's reference vector and the input record. Euclidean distance is equal to the square root of the squared difference between a reference vector (node) and an input (obs), summed over the total number of grid points (Eq. 2.1).

$$Dist_{Euclidean} = \sqrt{\sum_{n=1}^{\#\ grid\ points} \left(SLP_{node_n} - SLP_{obs_n}\right)^2} \qquad \text{Eq. 2.1}$$

The node with the smallest Euclidean distance from a given input record is labeled the "winning node."

The weight of the reference vector for the winning node—and thus, the position of the node—is adjusted by a user-specified learning rate to better represent the input data. This learning rate is a small value that essentially produces a fraction of the distance between the reference vector weight and the input record. So, the weight of the reference vector is adjusted to become the sum of its old weight and the new fraction created by the learning rate. The basic adjusted reference vector ($node_{n+1}$) is equal to the difference between the input (obs) and reference vector ($node_n$), multiplied by a user-specified learning rate L, and added to the original reference vector (Eq. 2.2). The subscript n denotes the iteration.

$$node_{n+1} = node_n + L_n(obs_n - node_n) \qquad \text{Eq. 2.2}$$

As the program progresses, the nodes become better representatives of the SLP patterns from the input, and they require finer adjustment, so the learning rate is decreased with each iteration. The learning rate L is decreased by multiplying by an exponential of the iteration (n) divided by a time constant (λ) that is dependent on a neighborhood (SOM space grid size—7X5 in this case), and the number of times—or "runs"—the process is set to repeat (Eq. 2.3). A range of learning rates were tested and showed little difference in the final results.

$$L_{n+1} = L_0 * exp^{\frac{-n}{\lambda}}$$ Eq. 2.3

The winning node does not get adjusted independently of all of the surrounding nodes. Since all of the nodes represent a continuum of the most typical patterns of SLP, the nodes that surround the winning node are related, and thus must also be adjusted, though proportionally less. This is done through the use of the neighborhood function (Eq. 2.4).

$$\theta_n = exp^{-\frac{dist^2}{2\sigma_n^2}}$$ Eq. 2.4

To establish the neighborhood function (θ), first define a neighborhood σ . This radius generally starts very large, often as the distance across all of the nodes (begins at 7X5 for this study), and then decreases with each iteration. The Euclidian distance is denoted by "dist" in Equation 2.4. So, the neighborhood becomes any node within the defined radius around the winning node. The result is that progressively fewer nodes are adjusted, until the only node adjusted is the winning node. In this study, the radius follows a Gaussian profile so that the nodes closest to the winning node are adjusted the most, and the nodes furthest away are adjusted very little, if at all. The radius also decreases linearly as the runs progress.

The full adjustment process then is determined by the distance between the reference vector and the input record, a learning rate that adjusts the winning node, and a neighborhood function that adjusts all of the nodes within a given radius around the winning node. The full, adjusted reference vector ($node_{n+1}$) is computed by adding the reference vector ($node_n$) to a quantity of a neighborhood function θ , multiplied by the learning rate (L), multiplied by the difference between the input (obs) and reference vector ($node_n$) (Eq. 2.5).

$$node_{n+1} = node_n + \theta_n L_n(obs_n - node_n)$$ Eq. 2.5

The run is complete when all input records have been compared to each node's reference vector. The final weight of each node's reference vector at the end of each run is then set as the initialized weight for the next run. This is done to help the nodes converge more efficiently. The entire process is completed when the nodes become sufficiently similar to themselves between runs. In this study, the process takes about 5,000 runs, but this will change depending on the data being used.

The final placement of the maps in the SOM space represents a position approximating the mean of nearby samples in the data space. SOMs will place dissimilar maps farther apart, and similar maps closer together.

The vocabulary describing SOMs is not entirely universal, and changes from paper to paper. So, for clarity, the following terms will be used consistently within this thesis. "Input" describes the observed SLP data that determine the initial nodes, and are compared with the nodes as the program progresses. "Iteration" refers to each time a node is compared to a day in the input data series. A "run" refers to the entire process of comparing the nodes to each day in the input data series, adjusting the winning node, and producing a final map space. 'Convergence' refers to the point when nodes no longer change appreciably between runs.

SOMs produce a continuous collection of representative maps referred to as the SOM space, and this attribute lends itself to classification of synoptic patterns (Hewitson and Crane 2002). Continuous representation of data yields more information than methods where data is grouped into distinct categories, like empirical orthogonal functions (EOFs). So, more detailed analyses of prevailing patterns can be done. Other strengths, like the ability to fill gaps in incomplete data and to capture non-linearity also benefit studies in synoptic climatology. Additionally, the user can choose to produce a larger number of maps to represent the data continuum, allowing for much finer detail than other methods.

2.1.2 - Sensitivities and issues applying to climate projects

A feature of SOMs—that they assume data is continuous—is helpful for extrapolating for missing data, but can be problematic for data with genuine gaps, as the SOM will attempt to bridge it artificially. Unfortunately, there is little that can be done about this as it is a critical feature for SOMs, so care must be taken to check that the SOMs are correctly representing the input data (Hewitson and Crane 2002). Since SOMs produce a visual output, this check can be done mostly through visual inspection, by comparing the SOMs to observed maps, but if more detail is needed, checks based on Euclidean distance and correlations could also be used.

While SOMs allow the user to visually see the differences between nodes (different SLP patterns, in this case), they do not show if two adjacent nodes are more or less similar than a different set of adjacent nodes. This is an issue that can be addressed with some extra treatment at the end of the SOM program.

Once the SOM nodes are constructed, the Euclidean distance between each adjacent node can be calculated, and produce a distortion map, where again similar nodes are spaced closer, while less similar nodes are spaced further apart. This can be a useful visual treatment, and allows grouping of similar maps in order to more easily analyze a larger map space (Hewitson and Crane 2002).

It is also important to optimize both the number of runs and the number of maps necessary for the given analysis. Too few runs may not allow the maps to reach convergence, while too many runs will be inefficient. Too few maps will fail to capture the fine detail that is the strength of SOMs, but too many maps will be overwhelming and make it difficult to differentiate between maps. Finding a balance is easier with maps, since the final maps can be grouped afterward using spatial correlations (Mills and Walsh 2014). However, finding a balance with runs includes a large component of trial and error. This project began with a number higher than—but in the neighborhood of—numbers of runs referred to in several background references, resulting in a starting

number of 10,000. This number was then systematically decreased until the final output maps showed changes.

2.2 – Data

2.2.1 - NCEP Reanalysis

The dataset representing North Pacific atmospheric conditions is provided by the National Center for Environmental Prediction (NCEP) Reanalysis I (Kistler et al 2001). This project used daily global sea level pressure (SLP), over the North Pacific domain, 30N–70N and 145E–235E. The NCEP Reanalysis assimilates 4-times daily observations into a forecast model, on a 2.5 degree X 2.5 degree grid, spanning 1948-2014. The data was further aggregated into winter (NDJFM) and summer (MJJAS) periods. The SOMs maps have been calculated using daily values for all years during the winter season. SOMs were also constructed for a subset of winter years based on the phase of the PDO, and the NPM, as well as during the summer season for the NPM. Positive and negative phases of each oscillation were explored separately by compositing synoptic maps based on the phase.

2.2.2 – Climate index subsets

Each of the climate indices was separated by sign of the phase and then composited by taking either all, or just the strongest years for each phase. The years used in each subset are listed in Table 2.1. The subset for PDO and rPDO phases used the years defined for each phase by McAfee (2014). The years chosen for ENSO subsets were determined using SST anomaly data from the Climate Prediction Center (CPC), which was provided by the Earth Systems Research Laboratory (ESRL) at http://www.esrl.noaa.gov/psd/data/climateindices/list, and was retrieved in 2014. Both the central tropical and east central tropical SST regions are considered by using Niño4 (5N-5S, 160E-150W) and Niño3.4 (5N-5S, 170W-120W), respectively (Figure 2.1). Only years with an anomaly greater than one standard deviation above (El Niño) or below (La Niña) the mean were used in the ENSO subset.

Table 2.1 Years used in each of the climate index subsets

Positive PDO Years	Negative PDO Years
1970, 1977, 1981, 1983, 1984, 1985, 1986, 1987, 1988, 1994, 1998, 2003	1949, 1950, 1951, 1952, 1954, 1957, 1962, 1964, 1965, 1966, 1967, 1969, 1971, 1972, 1974, 1976, 1989, 1991, 1995, 2000, 2002, 2008, 2009, 2011
Positive rPDO Years	Negative rPDO Years
1977, 1981, 1984, 1985, 1986, 1987, 1988, 1994, 2001, 2003	1949, 1950, 1951, 1952, 1953, 1954, 1957, 1962, 1964, 1965, 1966, 1967, 1969, 1971, 1972, 1973, 1974, 1976, 1979, 1991, 1995, 1999, 2009, 2011
El Niño (3.4) Years	La Niña (3.4) Years
1958, 1966, 1969, 1973, 1983, 1987, 1992, 1995, 1998, 2003, 2010	1955, 1956, 1971, 1974, 1976, 1989, 1999, 2000, 2008, 2011
El Niño (4) Years	La Niña (4) Years
1958, 1966, 1969, 1973, 1983, 1987, 1988, 1992, 1995, 1998, 2003, 2005, 2007, 2010	1951, 1955, 1956, 1965, 1971, 1974, 1976, 1989, 1999, 2000, 2008, 2011
Positive NPM Years	Negative NPM Years
1958, 1962, 1963, 1986, 1987, 1991, 1992, 1994, 1996, 1997, 2005, 2014	1951, 1952, 1956, 1969, 1971, 1974, 1976, 1989, 1999, 2000, 2008, 2011, 2012, 2013
Big Fire Years	Small Fire Years
1950, 1957, 1969, 1977, 1988, 1990, 2002, 2004, 2005, 2009	1948, 1949, 1955, 1961, 1962, 1963, 1964, 1965, 1978, 1995

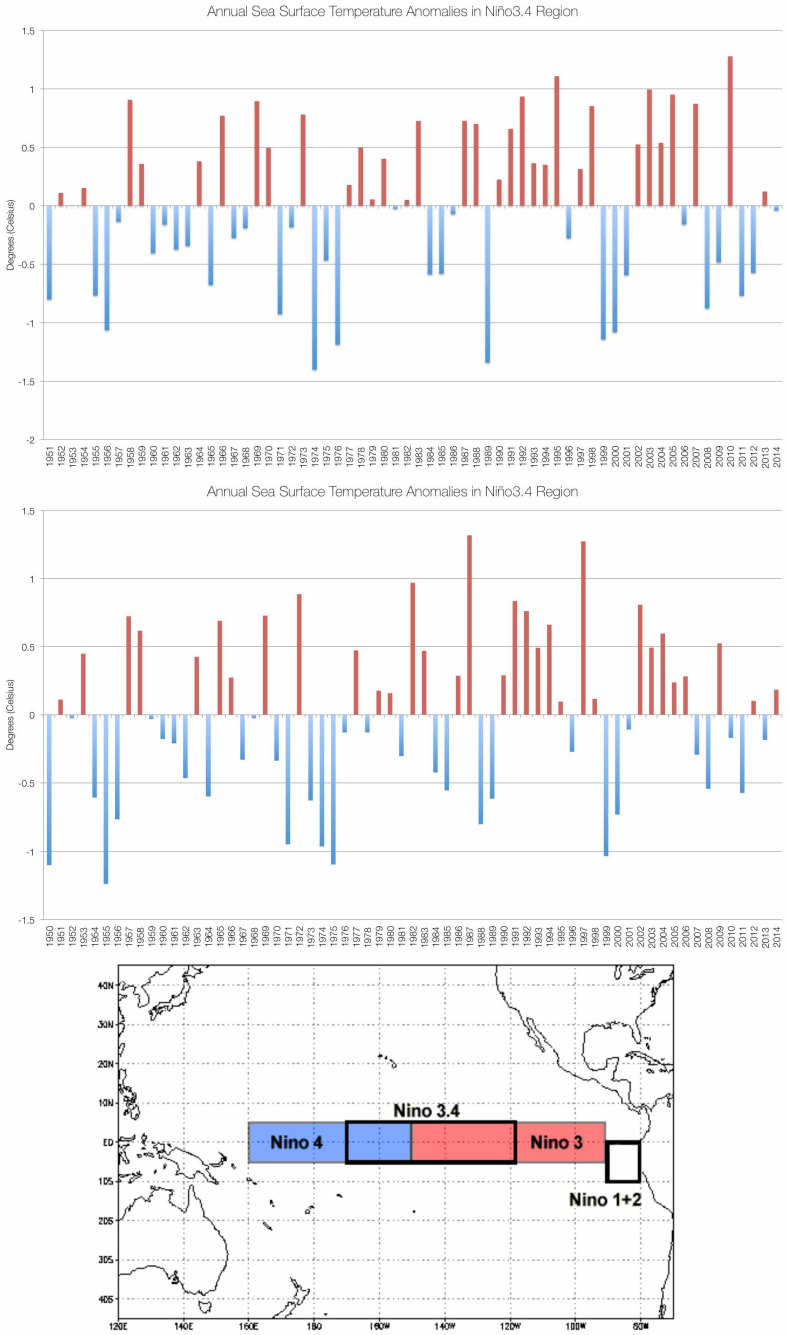

Figure 2.1 Top panel is the time series for SST anomalies in the Niño4 region. Middle panel is the same, but for the Niño3.4 region. Bottom panel is a map showing the location of El Niño regions. SST is in ˚C.

The NPM time series is based on the NOAA ERSST V3 sea surface temperature data provided by NOAA/OAR/ESRL PSD, from their website at http://www.esrl.noaa.gov.psd/, retrieved in 2014. The NOAA extended dataset is based

on simulated data from models and observations, as well as bias-adjusted AVHRR satellite SST data. This data was then averaged over the NPM region of the Pacific: 55N–45N and 150W–130W (Bond et al. 2015). Only years greater than one standard deviation from the mean were picked for the positive and negative NPM subsets.

2.3 – Application of SOMs

2.3.1 – Separating winter and summer

This study separated the daily SLP data into winter (NDJFM) and summer (MJJAS) subsets, and computed a SOM space for each season, in order to view the SOMs for each index in their strongest or most influential season. The PDO signal is only present in the winter. The NPM is present in both winter and summer. A very strong positive NPM in the winter preceded the record warm temperatures in 2014 in the winter. Additionally, positive summer NPM occurrences have preceded five out of the six big fire (> 3 Million acres burned) years during the period of record for this study (Figure 2.2).

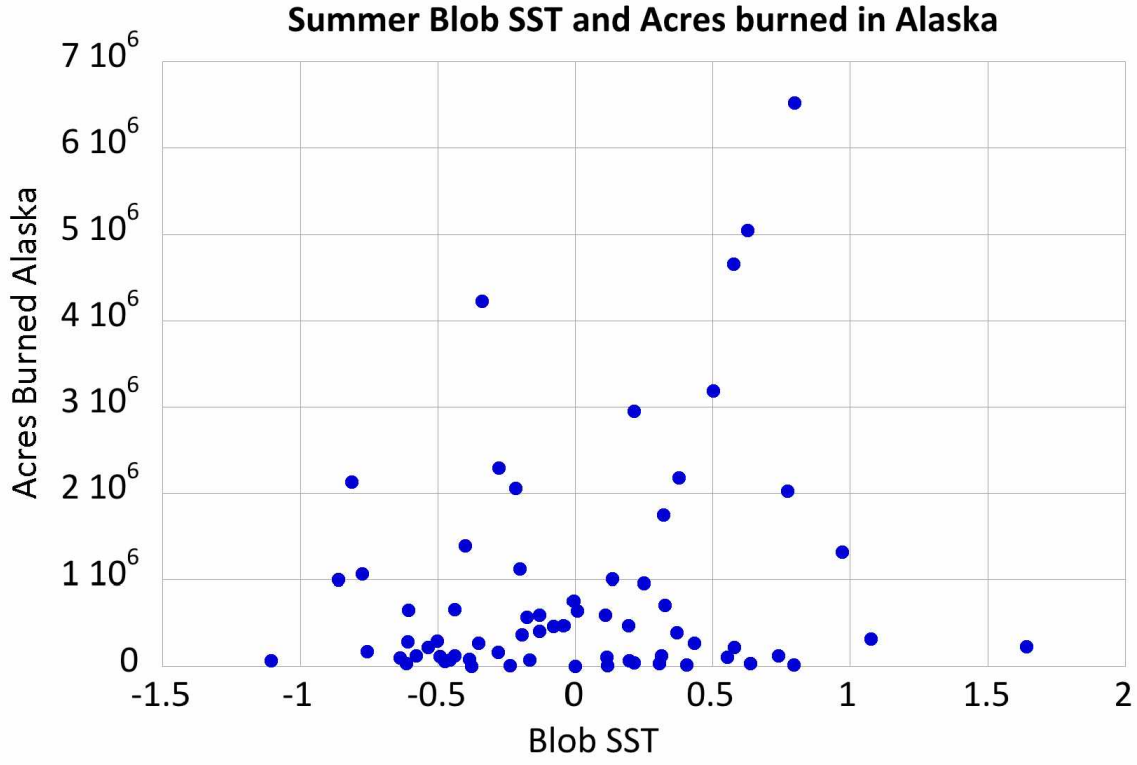

Figure 2.2 Scatterplot of summer NPM SST (degrees C) and acres burned in Alaska

2.3.2 – Measurements of error

In order to determine a metric for the performance of the SOMs as compared to the traditional climatology, two measures of error were produced. The first is the average error as defined by Euclidean distance, where the distance between a SOM node and its most closely matched SLP observation is summed for all of the nodes, over the entire number of days (9,982 in winter, 10,318 in summer). The second metric is defined by the average pattern correlation, which was computed for each of the 35 maps, comparing each map to its best matching SLP observation. The correlations are quite high, with the majority of maps having a correlation coefficient above 0.7. To define climatology, the method of pattern correlation was used again, but compared to the mean of all 35 maps, rather than the best matching SLP observation, where the mean of the 35 maps represents the climatological average. In this case, correlation coefficients were much lower, near zero. Figure 2.3 shows histograms of both pattern correlations. The much greater correlation when the maps are compared to the SLP observations suggests that the SOMs perform better than climatology when realistically representing the SLP observations.

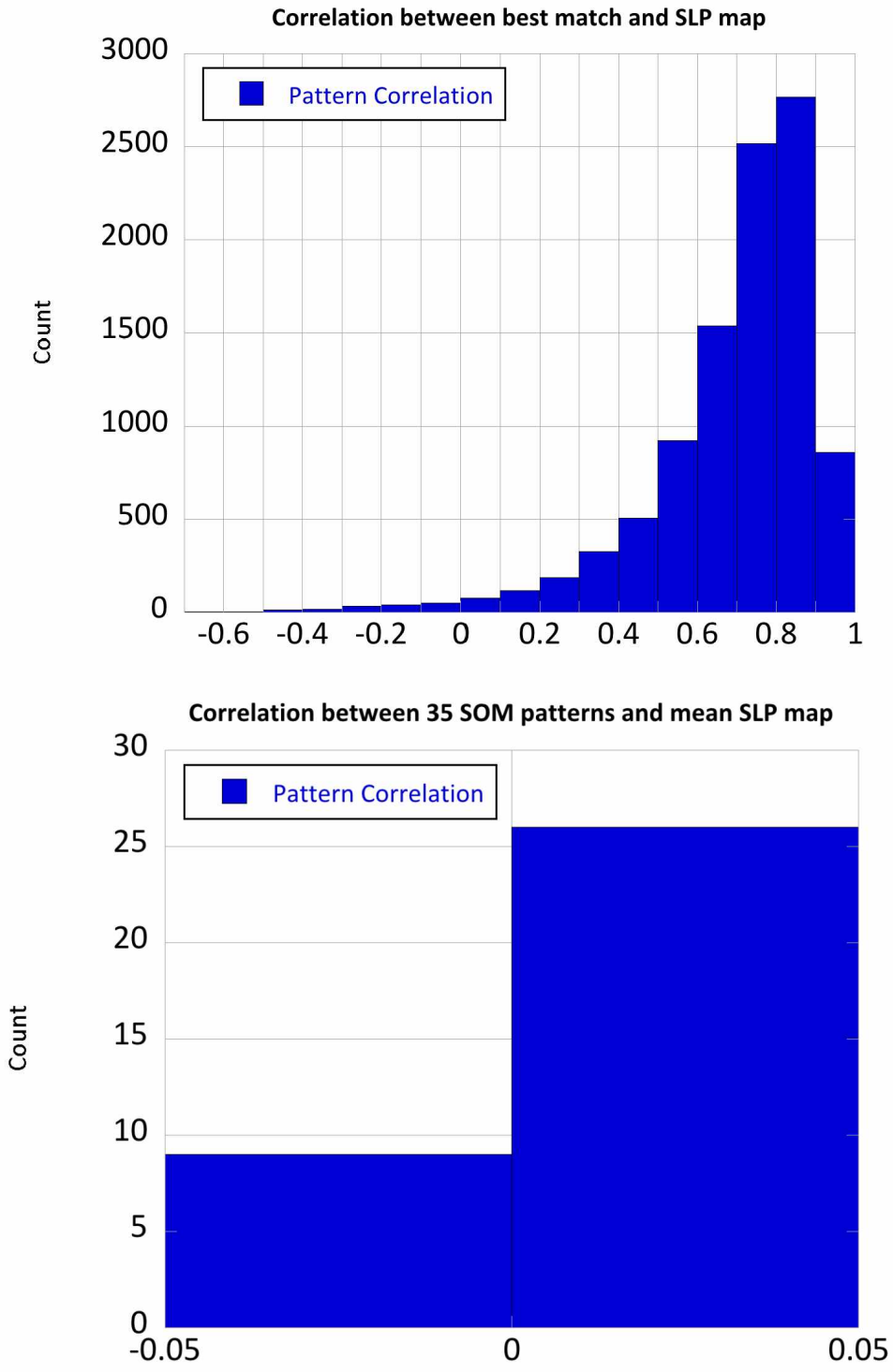

Figure 2.3 (top) Histogram of pattern correlations between each map in the SOM and the best matched SLP observation. (bottom) Histogram of pattern correlations between each map in the SOM and the average of all of the maps in the SOM.

Chapter 3 - Seasonal SOM patterns

Winter and summer synoptic patterns are investigated separately in this study over the 1948-2014 period using SOMs produced with daily SLP data from NCEP Reanalysis, November-March and May-September, respectively. Different climate indices and climate-related variations are explored for both seasons in an attempt to link the indices to the seasonal climate variability through their shared relationship with synoptic patterns.

3.1 – Winter

The most distinctive feature of the winter climatological SLP (Figure 3.1) for the North Pacific is a weak (~1004 hPa—though the low strengthens during the mid-winter months), but expansive low-pressure pattern, whose center spans almost the entirety of the North Pacific (42N-52N latitude, 155W-155E longitude).

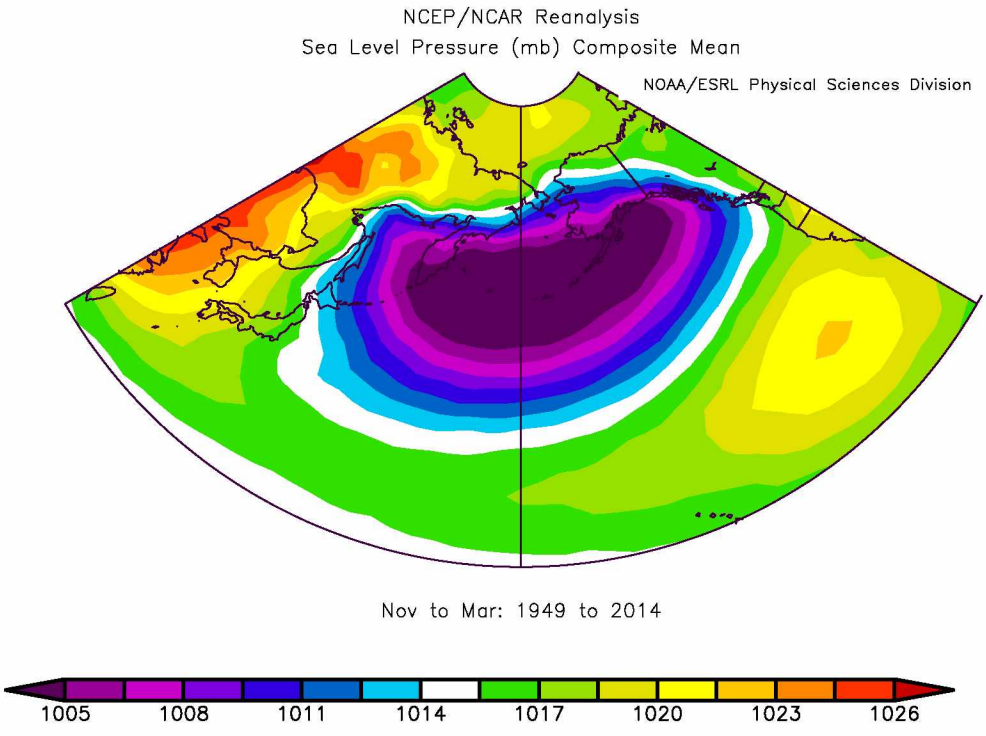

Figure 3.1 Mean sea level pressure for winter (Nov-Mar) over 1949-2014 in hPa. Data for this plot are from NOAA/ESRL, Boulder, CO, at http://www.esrl.noaa.gov/psd/; retrieved July 2015.

A subtropical high is also present, just off of the west coast of the contiguous US, as well as generally high pressure over Asia and Russia (Siberian High). For Alaska, the placement of the low-pressure pattern implies a climatological prevailing southeasterly flow. The climatology is represented by the mean SLP, and the Aleutian Low is a distinguishing feature of wintertime synoptic patterns in the North Pacific (Cassano and Cassano 2009). This seasonal climatological low pattern is present for the all-winter, positive and negative PDO, and positive and negative NPM but varies in intensity, generally becoming weaker in negative phase years.

The 7X5 array of SOMs (Figure 3.2) represents 35 types of synoptic patterns that occurred in the dataset of all winter days from 1949-2014.

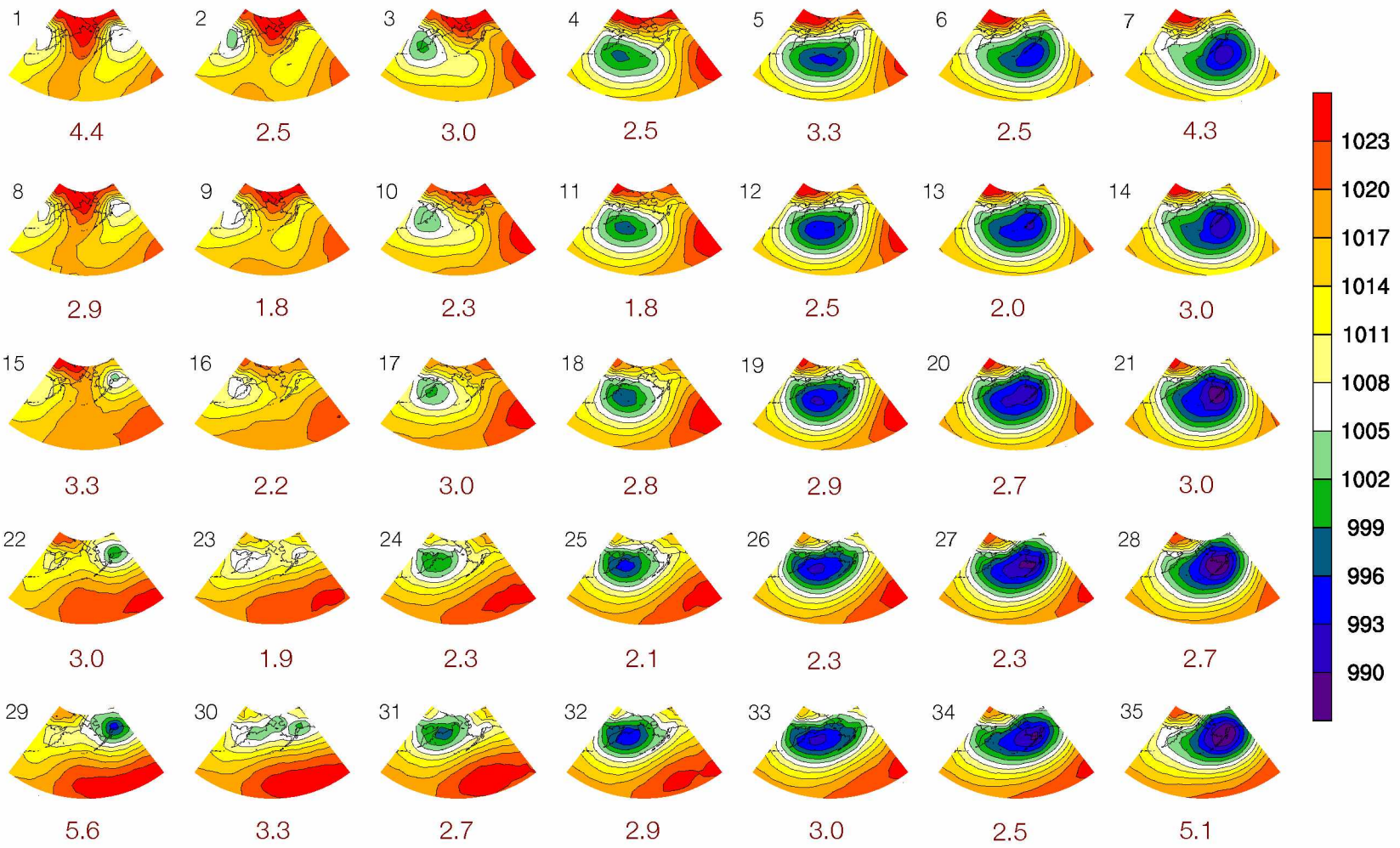

Figure 3.2 SOM space produced using daily SLP (in hPA) observations from NCEP Reanalysis for winter (Nov-Mar) 1949-2014. Number under each map refers to the percent of total daily SLP observations matched to the map (percent occurrence).

The number beneath each map is the percentage of all 9,982 total winter days that were matched to each map. This will be referred to as the 'percent occurrence' of each SOM.

Individually, the 35 SOMs have relatively uniform, low frequency. No map has a percent occurrence higher than 5.6%. As a group, patterns characterized by low pressure of varying strength comprised 78% of the daily SLP patterns in the all-winter dataset. The location of the low in these patterns also varies from the Bering Sea (39%), to the Aleutian Islands (30%), to coastal and Gulf of Alaska (9%), though most patterns locate the low over the Bering or Aleutians. The large region of relatively low pressure results from the passage of many slightly different low-pressure systems varying in strength and location in the North Pacific, rather than a more singular, persistent pattern.

High pressure, or ridge, dominated patterns are the minority in the all-winter SOM space. Just one corner of the SOM space is devoted to patterns characterized by the Beaufort High and a ridge over the Bering Sea, and represents 22% of the total observed winter patterns. However, there is still a strong influence of a subtropical high, even in some low-dominated maps. 86% of the observed patterns matched to a map with some presence of a subtropical high. Consequently, the subtropical high is distinctly visible in the mean, but the Beaufort high and Bering ridge are mixed into the ubiquitous high pressure in the Arctic, and Pacific basin, surrounding the low in the North Pacific.

The four individual maps with the highest percent occurrence are the maps at the corners of the SOM space. This may be because corner maps have to compete with only two similar maps to match with the observed patterns, while maps in the middle of the SOM space have to compete with three or four similar maps. So, the corner maps can match to observed patterns with a larger Euclidean distance (high error) than can a map in the middle of the SOM space. This poses the potential problem of high frequency, high error matches in the corners of the SOM space, elevating less precise maps, and weakening the representative ability of the SOM space. However, when the average error for each map (average Euclidean distance from the observed pattern) is

computed (Figure 3.3), the corner maps do not have the highest average error. Maps 1 and 7 are in the top five (2nd and 5th, respectively) maps with highest error, and map 28 is 12th, but map 35 is 22nd. The match strength is even more evident when the pattern correlation is computed between each SOM and the observed patterns matched to it (Figure 3.3). In this case, map 1 is the 8th weakest, map 7 is the 22nd weakest, map 28 is the 7th strongest, and map 35 is the strongest map overall. A problem of high error matches dominating the corners is not apparent in the SOM space used for winter.

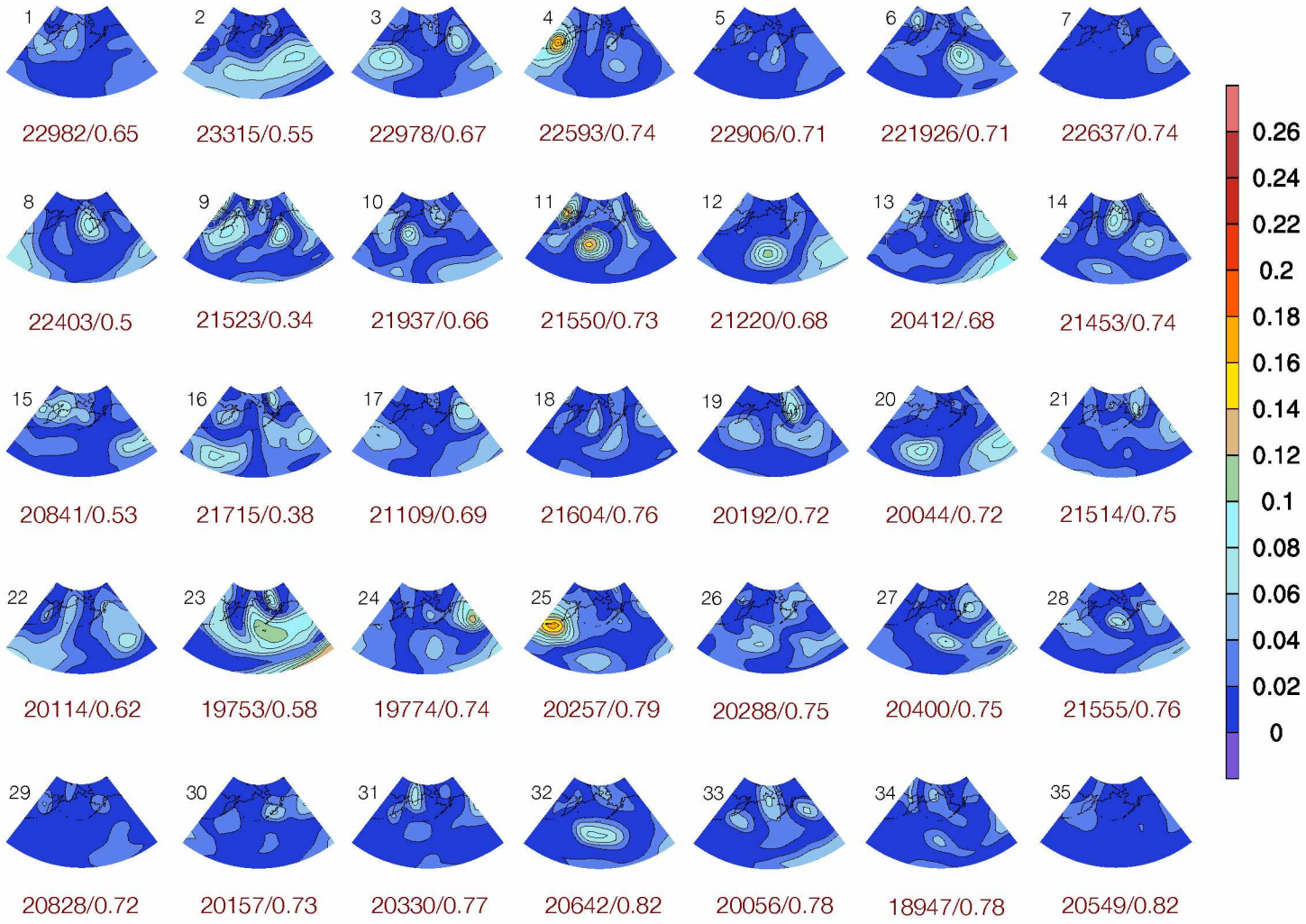

Figure 3.3 SOM Error computed using average Euclidean distance and average pattern correlation during All Winter Years (map units: hPa).

The corner maps are the most different maps from each other, so while they do not appear to be catching all of the weakly matched extreme patterns, they do represent the bounds of the SOM space. No low is weaker and further west than the low over Siberia, west of the Bering ridge in map 1, no low is further south than the low in map 7, no low is further north than the low over Alaska in map 28, and no map is stronger or further east than the low in map 35. Figure 3.4 focuses on the four corner maps. Map 1 shows two very weak low-pressure centers. One low-pressure center is over the western Pacific, and the other over the south-central coast of Alaska, and Gulf of Alaska. A tongue of strong high pressure drops south from the Arctic, creating a ridge over the Bering Sea. Map 7 shows a strong low-pressure system centered just south of the Aleutian Islands, and spanning much of the North Pacific. Map 29 has the highest frequency, representing 5.6% of the winter days from 1948-2014. It shows a small, circular low-pressure system over the Kenai Peninsula, and the south central coast of Alaska. Strong high pressure spans a large east-west swath south of the Gulf of Alaska and into the subtropics. Map 35 has a strong low centered on the Kenai Peninsula, and extends into Interior Alaska. Strong high pressure in the subtropical eastern Pacific creates a tight pressure gradient between the subtropics and the Interior of Alaska.

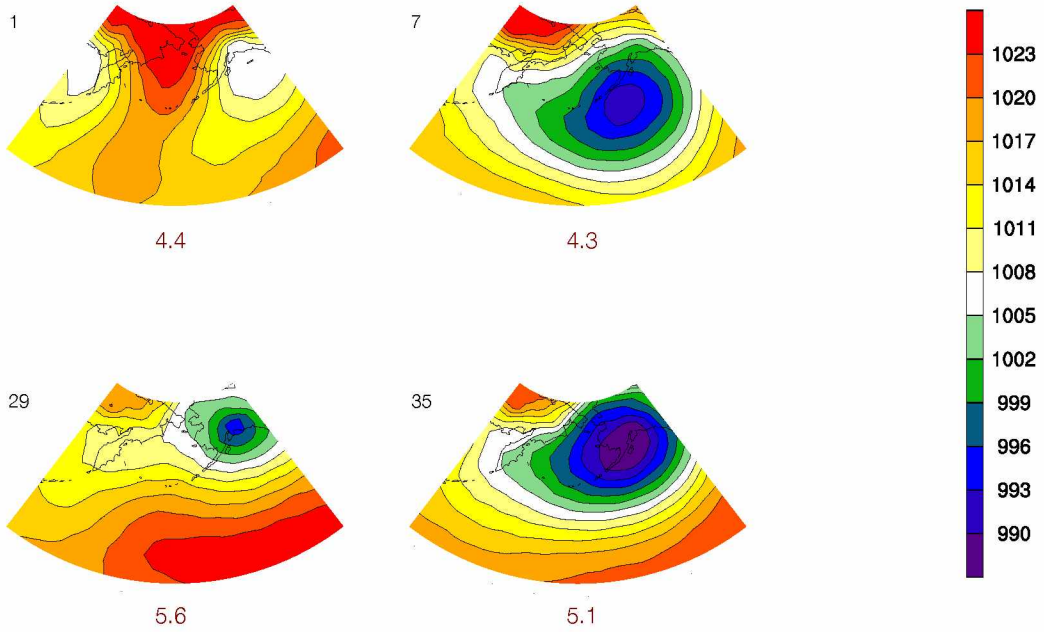

Figure 3.4 Four maps at the corners of the all-winter SOM space depicted in Figure 3.2. Contours are SLP in hPa.

3.1.1 – Pacific Decadal Oscillation

The climatology for positive PDO (Figure 3.5a) is the long term average of daily SLP observations from NCEP for only the years that occurred during the positive PDO phase (Table 2.1). The same technique was used to construct the climatology for negative PDO (Figure 3.6a). Both climatologies are compared to composite SLP anomaly maps for the same PDO years (Positive Phase: Figures 3.5b; Negative Phase: Figures 3.6b). All maps are consistent with the canonical PDO pattern (Figure 1.2).

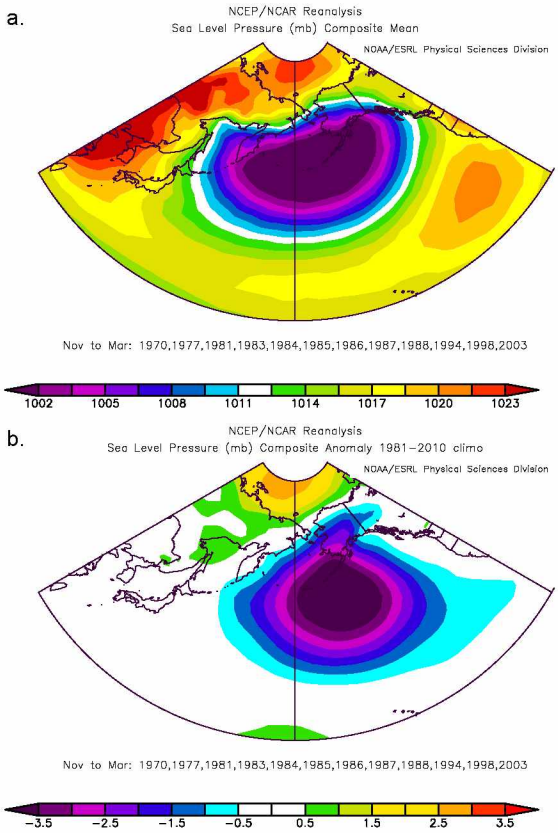

Figure 3.5 a. Sea level pressure (hPa) composite mean for positive PDO phase winter years (see Table 2.1) b. Sea level pressure (hPa) composite anomaly for positive PDO phase winter years. Data for this plot are from NOAA/ESRL, Boulder, CO, at http://www.esrl.noaa.gov/psd/; retrieved July 2015.

Positive PDO climatology shows a flattened oval of strengthened low pressure (998 hPa), centered over the Aleutian Islands with prevailing southeasterly flow over Alaska. The shape of the low-pressure patterns in the mean SLP maps for all indices in the winter are similar, even within the same phase. The primary distinguishing feature that differentiates each phase is the relative strength of the SLP patterns. The low in the

positive phase of PDO is stronger than the low in the all-winter and the negative phase. This produces the low SLP anomaly generally associated with the positive phase of PDO. The Aleutian Low in the anomaly results in southerly flow into Alaska, suggesting a higher prevalence of patterns with southerly flow during positive PDO years. This is also consistent with the canonical description of the positive phase of the PDO.

The climatology for the negative phase of PDO shows a weak region of low pressure (1004 hPa) (Figure 3.6a). High pressure (1008 hPa) over the Aleutian Islands pinches the region to create an almost separated large area over the western Pacific, and a smaller area located in the Gulf of Alaska. The higher-pressure area is responsible for the high SLP anomaly that is associated with the canonical negative phase of PDO, which shows anomalous high pressure over the Aleutians. When compared with the strong Aleutian Low during the positive PDO, this synoptic pattern visually establishes the difference between the synoptic conditions of positive and negative phases of the PDO.

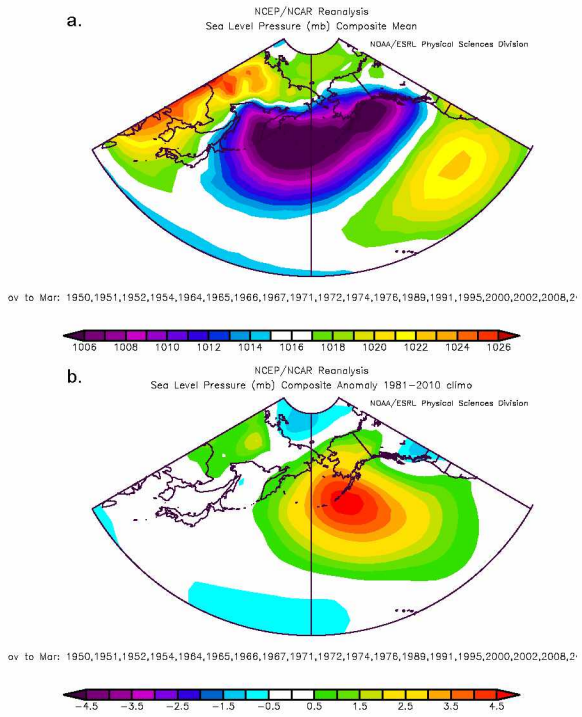

Figure 3.6 a. Sea level pressure (hPa) composite mean for negative PDO phase winter years (see Table 2.1) b. Sea level pressure (hPa) composite anomaly for negative PDO phase winter years. Data for this plot are from NOAA/ESRL, Boulder, CO, at http://www.esrl.noaa.gov/psd/; retrieved July 2015.

Climatology suggests the positive PDO phase favors low-pressure patterns. To find which specific winter SLP patterns were favored most by each phase of PDO, the percent occurrence was calculated for each map in the winter SOM space, using only daily SLP observations from positive or negative PDO years. The difference in percent occurrence between the positive and negative phase for each map is computed by subtracting the negative phase percent occurrence for each map from the positive phase percent occurrence. A large difference for a given map implies that the map is favored one of the phases. Any difference greater (less) than, or equal to, one standard deviation (1.4 percent occurrence) above (below) the mean difference (0.0) is labeled as being favored by the positive (negative) phase in Figure 3.7. Five (six) maps exceeded one sigma for the positive (negative) phase of the PDO. The remaining 30 maps (29 for negative PDO) do not change dramatically between phases, suggesting their presence under all conditions.

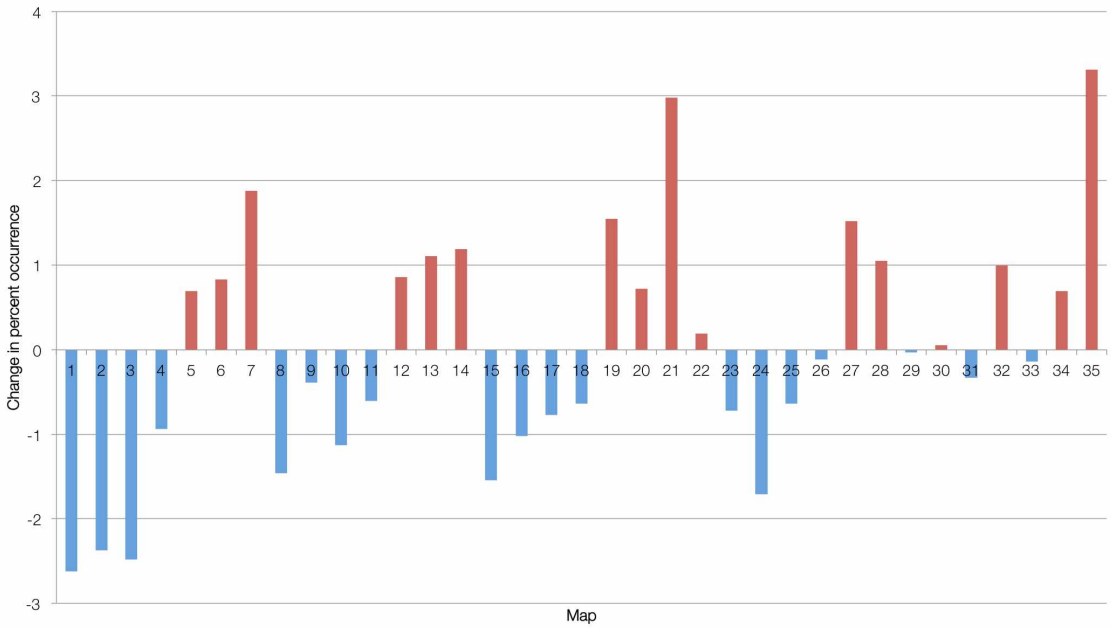

Figure 3.7 Difference in percent occurrence (positive – negative) between phases of PDO.

Five maps exceed one standard deviation above the mean phase change: 7, 19, 21, 27, and 35 (Figure 3.8). All five maps show a strong low-pressure system in the western Gulf of Alaska, in the Bering Sea, or over the Kenai Peninsula and Aleutian Islands. The low is a similar shape in maps 7, 21, and 35, where there is a strong low center near Alaska, with the pattern extending west across the North Pacific. However, the exact centers of the lows are located in slightly different areas. Map 7 has the low in the western Gulf of Alaska, while the lows in maps 21 and 35 are progressively further north, over the Aleutians and Kenai, and over the Kenai and much of southern Alaska, respectively. Map 27 features a slightly flattened version of the low in map 21, with similar placement. The low in map 19 encompasses most of the Bering Sea. With the exception of map 7, the lows in all maps are oriented so that flow into Alaska is either southerly or southwesterly. In contrast, the low in map 7 suggests a more southeasterly flow over most of Alaska.

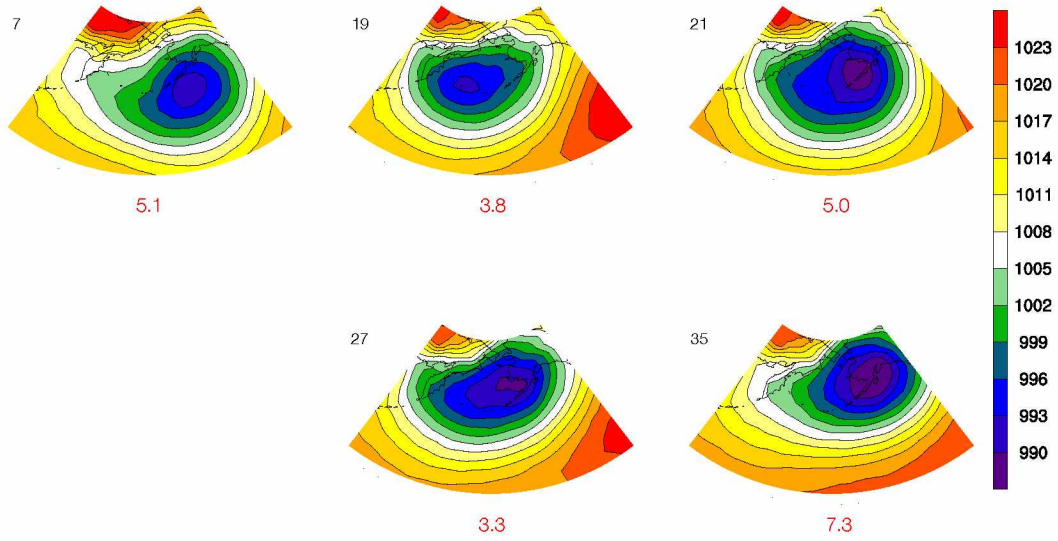

Figure 3.8 Maps from all-winter SOM space (see Figure 3.2) that are most favored by the positive phase of PDO. Map displays SLP in units of hPa.

The presence of strong low pressure in the region around the Aleutians is in agreement with the canonical description of the positive phase of PDO. Most maps are also consistent with anomalous warm temperatures in Alaska, generally associated with the positive phase of PDO. Southerly, and southwesterly flow suggests relatively warm marine air being brought into Alaska, with enhanced warming of the Interior resulting

from the Chinook winds, where humid air warms due to adiabatic compression after crossing the Alaska Range and losing altitude as it enters Interior Alaska. However, the southeasterly flow in map 7 would not necessarily result in the same effect, as this flow may include cooler, drier, continental air, and much less flow over the Alaska Range, and therefore would not be able to have as significant a warming effect. All five maps are of the strength and general location suggested by the canonical description of PDO, but one out of the five may cause very different temperature profiles for Alaska. This is a subtle difference that may get smoothed over when one pattern is used to describe all five patterns as is done with a composite anomaly map or an EOF.

Six maps exceed one standard deviation below the mean phase change: 1, 2, 3, 8, 15, and 24 (Figure 3.9). Except for maps 3 and 24, all the maps show a weak low, centered over the western North Pacific and Siberia, and an area of weak, relatively low pressure centered in the Gulf of Alaska, with a moderate-to-strong ridge extending from the Arctic between the lows. Maps 3 and 24 show a slightly stronger low over Siberia, but no area of low pressure near Alaska. All six maps would produce generally weak easterly flow over most of Alaska, setting up the persistent conditions that would result in anomalously low temperatures associated with the canonical negative phase of the PDO. However, maps 1, 8, and 24 map include an area of weak southerly or southwesterly flow near the south central coast of Alaska that could result in warmer, wetter conditions, at least near the coast. So, half of the maps favored by negative PDO would result in conditions more closely related to the positive phase for some parts of Alaska.

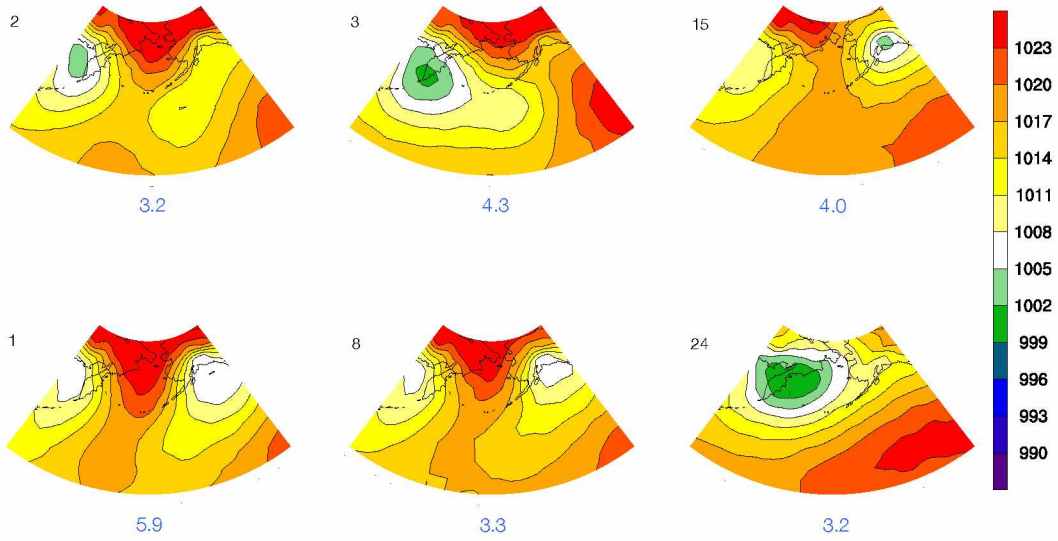

Figure 3.9 Maps from all-winter SOM space (see Figure 3.2) that are most favored by the negative phase of PDO. Map displays SLP in units of hPa.

To see the pattern distribution in each phase of PDO, and evaluate how truly representative the favorable maps were of the patterns in each phase of the PDO, SOM maps were constructed using only daily winter data that was characterized by positive or negative PDO years (see Table 2.1). The positive PDO SOM space (Figure 3.10) is dominated by patterns with strong low pressure varying in position from east and west of the Aleutian Islands (89% of observations), as well as a small number of patterns that show a ridge over the Aleutians (11% of observations). No maps show any southward extension of the Beaufort High. The correlation is then computed between each of the favorable maps and each of the maps within the positive or negative PDO year SOM space. The favorable patterns represent any map that has a correlation coefficient of 0.75 or higher. The five patterns that favor the positive phase of PDO represent 88% of the patterns that establish the positive PDO SOM space. This study focuses mainly on "favored" and "representative" maps because they are the only maps that are both one sigma above the mean difference in percent occurrence between phases, and have a correlation greater than 0.75 with maps in the SOM space that they represent.

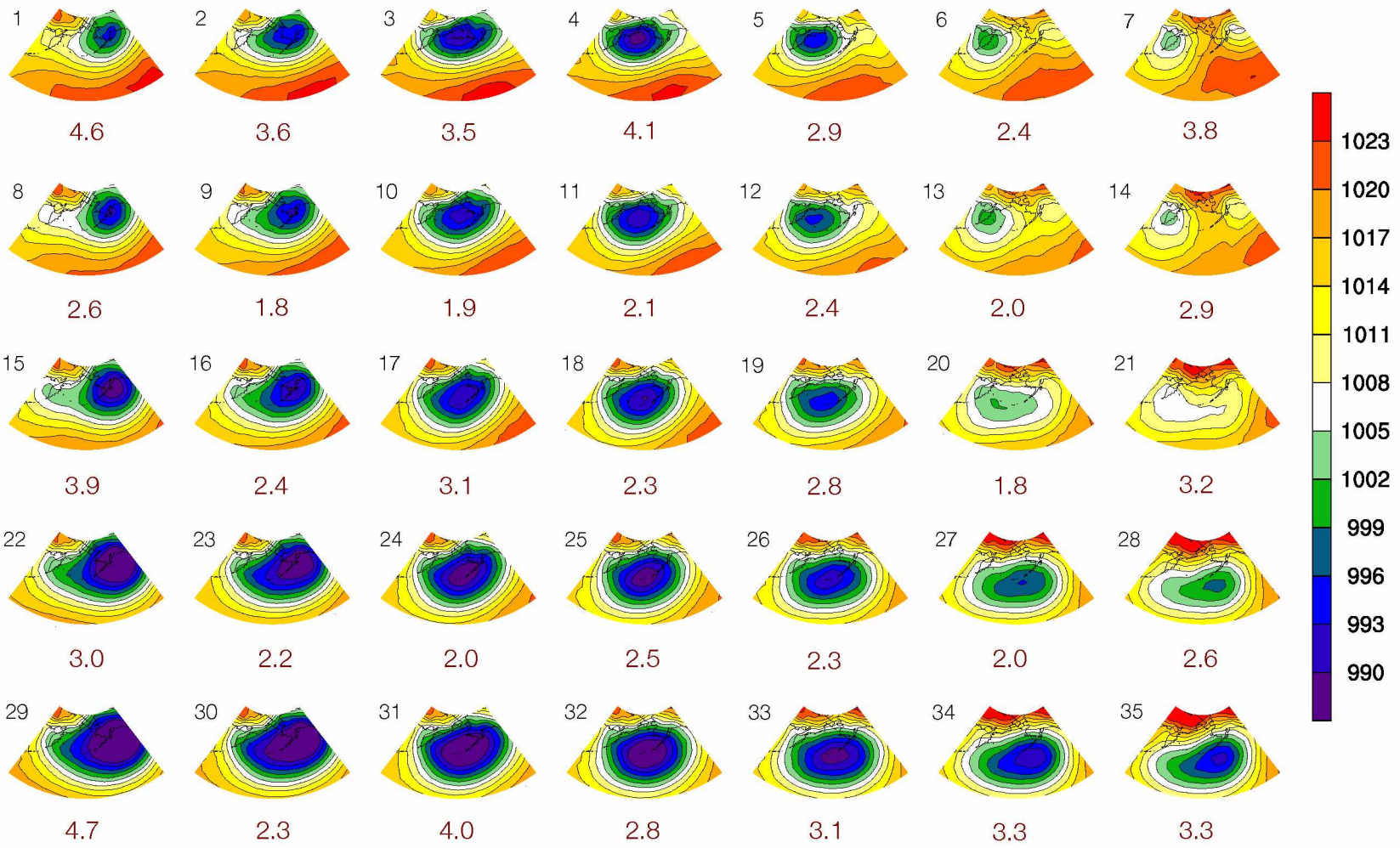

Figure 3.10 SOM space produced using daily SLP (in hPa) observations from NCEP Reanalysis for positive PDO phase winter years (see Table 2.1). Number under each map refers to the percent of total daily SLP observations matched to the map (percent occurrence).

As expected, patterns with a ridge are more prevalent in a SOM space produced using only PDO negative years (Figure 3.11). The lows in the Bering Sea are also generally weaker in the negative PDO SOM space, and there is a much more noticeable presence of both the Beaufort High, and the subtropical high and west coast ridging. However, maps with moderate-to-strong lows positioned near the Aleutian Islands still represent 61% of the SLP patterns during the negative phase. The six patterns that favor the negative phase of PDO represent 79% of the patterns that establish the negative PDO SOM space. The lower representation of the six patterns during the negative phase is likely due to the still strong presence of positive phase-like patterns during negative PDO years. This principle is more evident when comparing the favorable patterns to the SOM space of the opposite phase using the same pattern correlation analysis. When the six favorable patterns for the negative phase of PDO are correlated with the positive phase SOM space, the six patterns are shown to represent 45.3% of the patterns that determine the positive phase SOM space. So, almost half of the patterns associated with the positive phase of PDO are represented by the most typical negative phase patterns.

The change in pattern distributions between phases is responsible for the polarity when considering the SLP anomalies associated with canonical PDO, but the patterns most associated with the opposite phase maintain a presence in both SOM spaces. The polarity is achieved because the positive phase of PDO strongly favors the low-dominated corner of the winter SOM space, while the negative phase does not. However, the negative phase does not favor the opposite corner with the same strength. Rather, the negative phase might be better described as just having few instances that match the maps in the low-dominated corner.

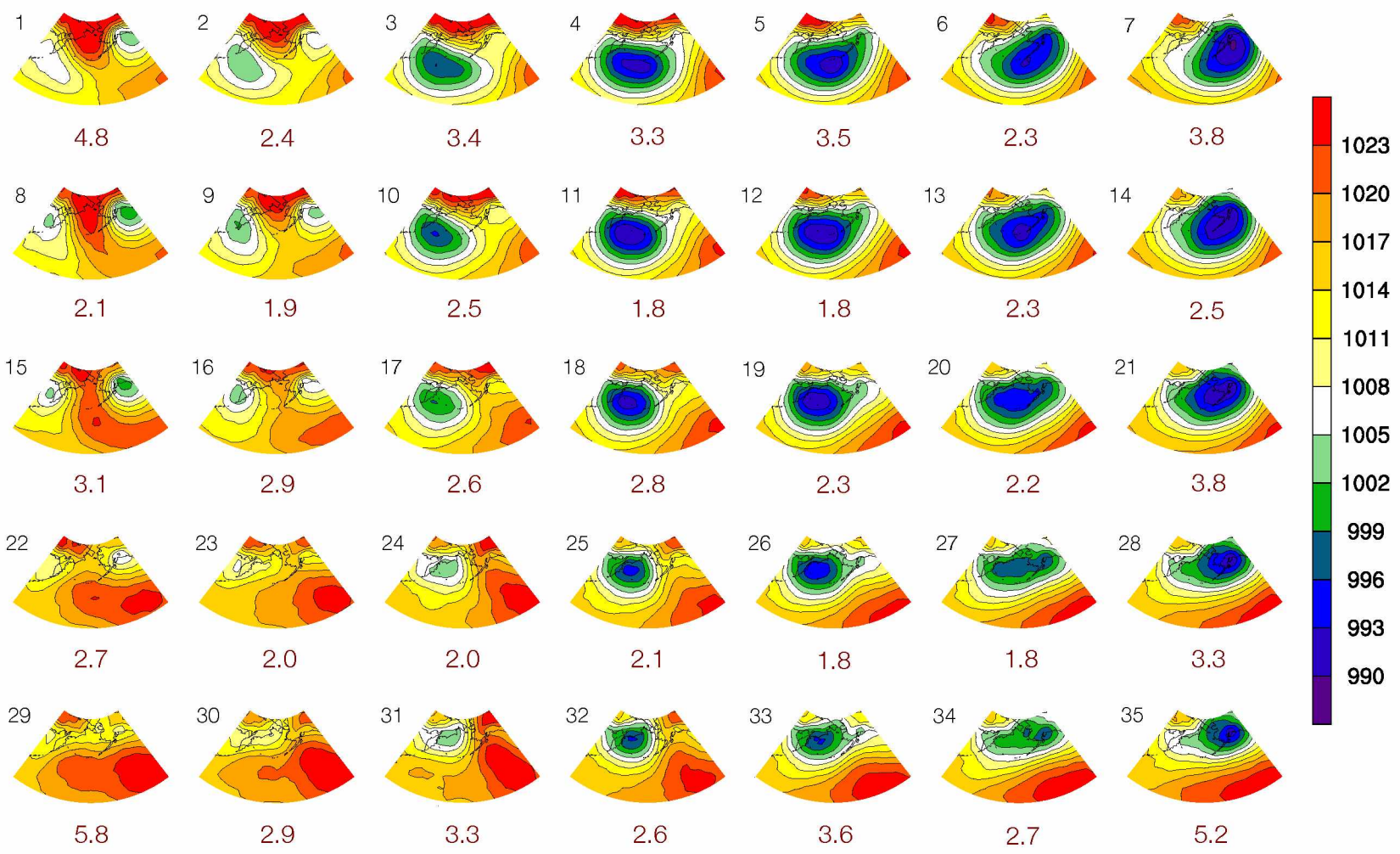

Figure 3.11 SOM space produced using daily SLP (in hPa) observations from NCEP Reanalysis for negative PDO phase winter years (see Table 2.1). Number under each map refers to the percent of total daily SLP observations matched to the map (percent occurrence).

3.1.2 - Residual PDO

To produce a more pure PDO signal, McAfee (2014) removed the ENSO variability from PDO by removing the Niño3.4 variability, and constructed the residual PDO (rPDO). While rPDO includes most of the same years for each phase as PDO, there are some differences (see Table 2.1). When only years for the positive or negative phase of rPDO are used to construct SOMs, similar to the method used for the PDO, the resulting patterns change slightly compared to when the standard PDO years are used.

Of the original five favorable maps that were produced using positive PDO years (7, 19, 21, 27, and 35), only maps 7, 19, 27, and 35 remain one standard deviation (1.2) above the mean (0.0). Map 21 drops out, and is replaced by map 32 (Figure 3.12). Map 32 has a strong low over western Bering Sea, and a strong region of high pressure in the eastern North Pacific. There is also weak high pressure over the eastern half of Alaska, generally westerly flow over the Gulf of Alaska, and weak southwesterly flow onto the southern coast of Alaska.

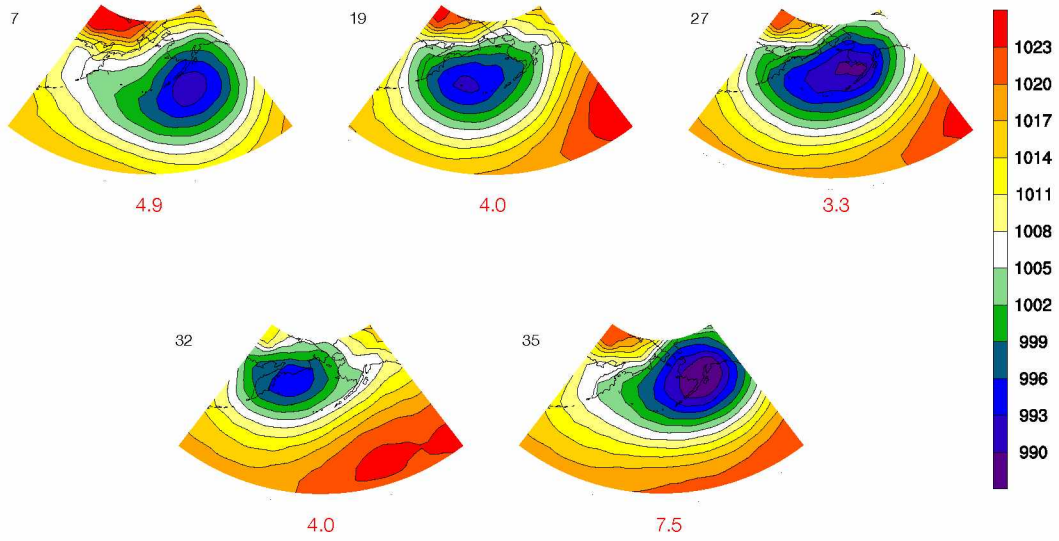

Figure 3.12 Maps from all-winter SOM space (see Figure 3.2) that are most favored by the positive phase of rPDO. Map displays SLP in units of hPa.

The exclusion of map 21 suggests that the pattern in map 21 may be governed by the eastern ENSO 3.4 signal. When the phase change analysis is performed using El Niño years (Figure 3.13), map 21 is identified as one of the maps that is more favored during

El Niño. The inclusion of map 32 suggests that map is influenced by some signal within rPDO only. Maps 7 and 35 are favored by the positive phases of PDO, rPDO, and ENSO, implying the strong signal of these patterns generally.

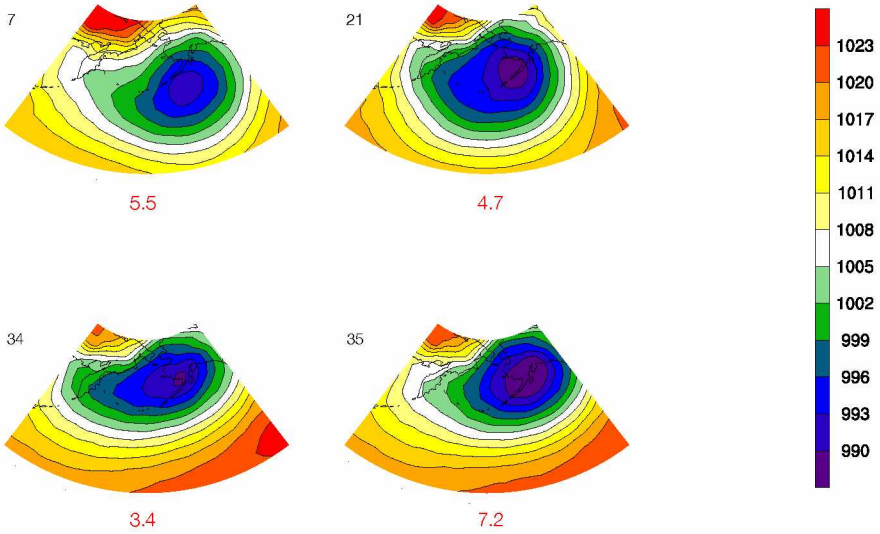

Figure 3.13 Maps from all-winter SOM space (see Figure 3.2) that are most favored by the El Niño (as defined using Niño3.4). Map displays SLP in units of hPa.

Of the original six maps produced using negative PDO years (1, 2, 3, 8, 15, and 24), only 2, 3, and 24 remain (Figure 3.14). Again, the exclusion of maps 1, 8, and 15 suggests that they are influenced by the ENSO signal, and this is supported by the appearance of both maps when this analysis is performed using La Niña years (Figure 3.15).

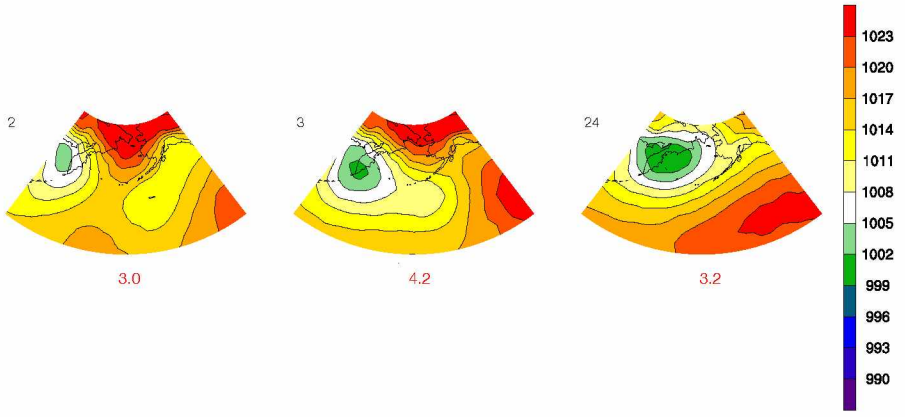

Figure 3.14 Maps from all-winter SOM space (see Figure 3.2) that are most favored by the negative phase of rPDO. Map displays SLP in units of hPa.

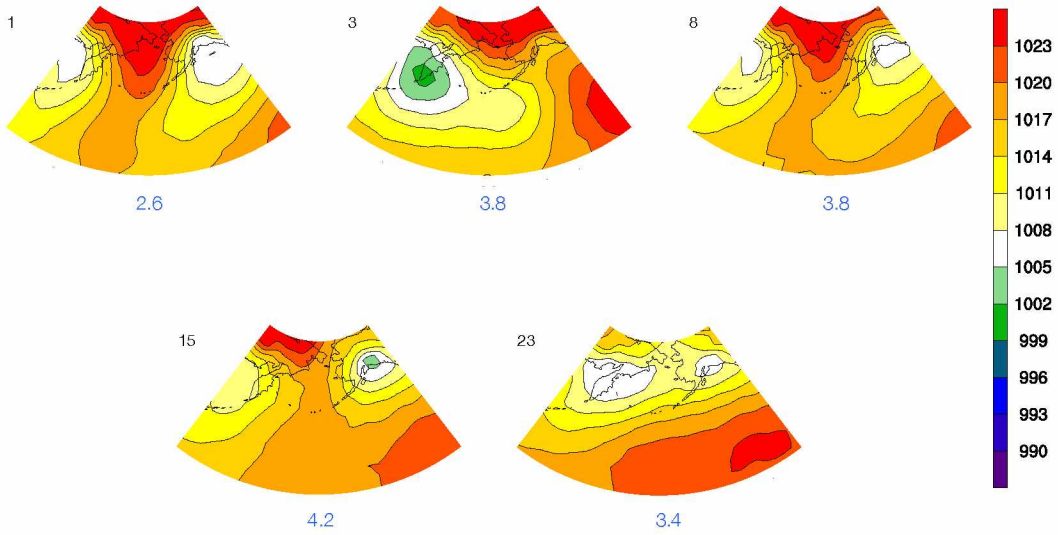

Figure 3.15 Maps from all-winter SOM space (see Figure 3.2) that are most favored by the La Niña (as defined using Niño3.4). Map displays SLP in units of hPa.

Originally, rPDO was to be included in this study as a potential, more "pure" replacement for PDO, but an analysis using pattern correlations, similar to PDO above, shows a more interesting attribute of rPDO. The five patterns that favor the positive phase of rPDO represent 88% of the patterns in the positive rPDO SOM space, while the three patterns that favor the negative phase represent 51% of the patterns in the negative rPDO SOM space. Additionally, the opposite phase correlation analysis shows that the three patterns favoring the negative phase represent 60% of the patterns in the positive rPDO SOM space. In contrast, the six maps that are favored by the negative phase of PDO only represent 45% of the positive phase of PDO. The flipped representation using the maps favored by the negative phase is only present in rPDO. This may be because the ENSO signal is a very distinct, organized signal. Therefore, its patterns will be more obviously represented in the mix of patterns comprising the PDO signal. Once it is removed, weaker, less distinctive signals, or mid-latitude processes receive relatively more representation, resulting in a somewhat more mixed signal.

3.1.3 – North Pacific Mode

Bond et al. (2015) documented anomalously warm water in the northeast Pacific (55N-45N and 150W-130W) starting in 2014 and continuing into 2015, and the climate anomalies associated with this warm water, which is being called the 'Pacific warm blob,' or North Pacific Mode.

When the maps favored by the positive NPM are extracted, there are three maps that exceed one standard deviation (1.2) above the mean (0.0): 7, 12, and 21 (Figure 3.16). Maps 7 and 21 feature a low-pressure system centered in the western Gulf of Alaska, and over the Kenai Peninsula, respectively. Both maps show little to no presence of high pressure in the eastern North Pacific. The low in map 12 is shifted further west, over the Aleutians Islands and Bering Sea, with a relatively strong ridge of high pressure over the eastern North Pacific.

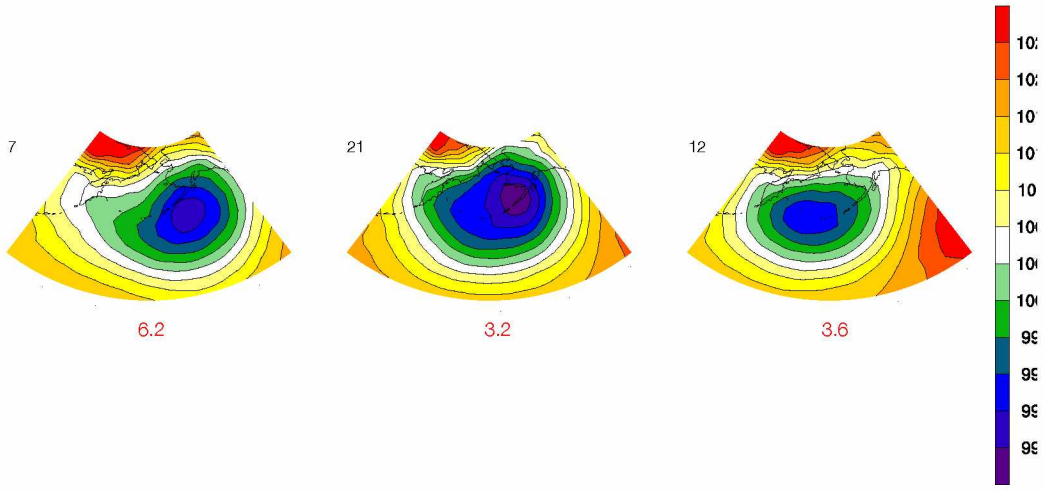

Figure 3.16 Maps from all-winter SOM space (see Figure 3.2) that are most favored by years with a positive NPM. Map displays SLP in units of hPa.

When the analysis focuses on only years associated with negative NPM events, five maps exceed one standard deviation below the mean: 1, 8, 15, 22, and 29 (Figure 3.17). Maps 1, 8, and 15 describe the same weak lows over Siberia and coastal Alaska, with a moderate-to-strong ridge over the Bering Sea from an extended Beaufort High that were prominently featured in the negative phase of PDO. However, maps 22 and 29 show a stronger low pushing well into Alaska, and an area of strong high pressure in

the eastern Pacific extending from the subtropics. This produces a tight north-south pressure gradient, with generally south and southwesterly flow into Alaska.

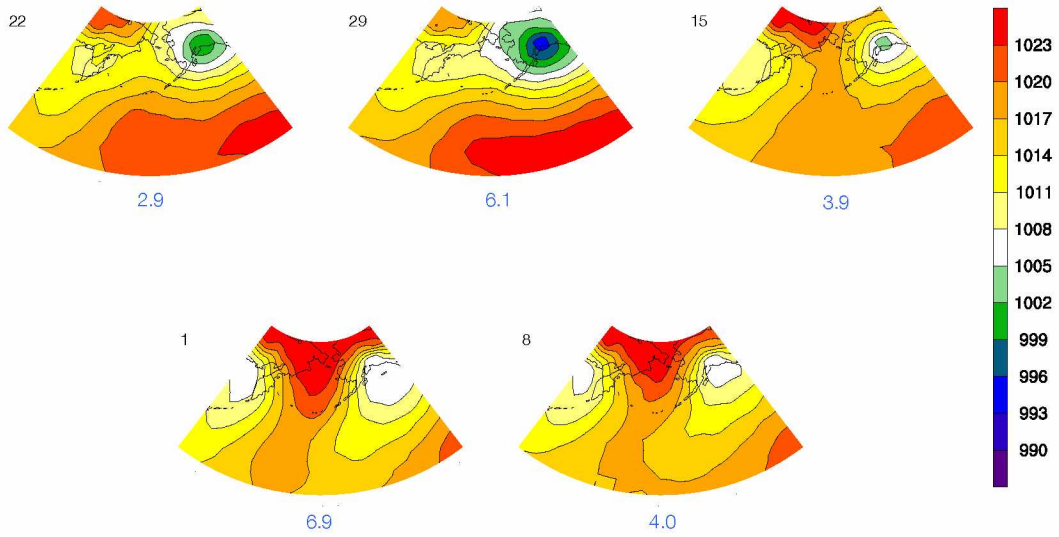

Figure 3.17 Maps from all-winter SOM space (see Figure 3.2) that are most favored by years with a negative NPM. Map displays SLP in units of hPa.

Initially, the resulting maps from this analysis of the NPM are confounding, particularly for the positive NPM. Two out of the three maps (7 and 21) do not closely resemble the SLP signature of anomalous high pressure in the eastern Gulf of Alaska (Bond et al. 2015). However, many of the maps from both phases are also maps that are favored when only ENSO years are considered in the analysis, suggesting the possibility that those maps represent the ENSO signal, as was the case for PDO. If only maps that are not also favored by ENSO are considered, the single resulting map when considering only positive NPM years would be map 12. This map includes strong high pressure in the eastern North Pacific, and ridging over the West Coast of the US, so it is much more representative of the SLP signature associated with positive NPM events. The two resulting maps when considering only negative NPM years would be 22 and 29. These two maps have low pressure positioned over coastal Alaska, resulting in more easterly flow into the Interior, likely producing cooler than normal temperatures. They also have more zonal westerly flow into the west coast of the contiguous US, indicative of cooler, wetter air than that associated with flow during the 2014 positive NPM conditions.

The SOM space created using only positive NPM years is mostly occupied by patterns with a moderate-to-strong low over the Aleutian Islands or Bering Sea, and no obvious dominance of a pattern with high pressure over the eastern Gulf of Alaska. About half of the maps show the presence of high pressure from the subtropics, and seven maps show at least some extension of the Beaufort High into the region (Figure 3.18).

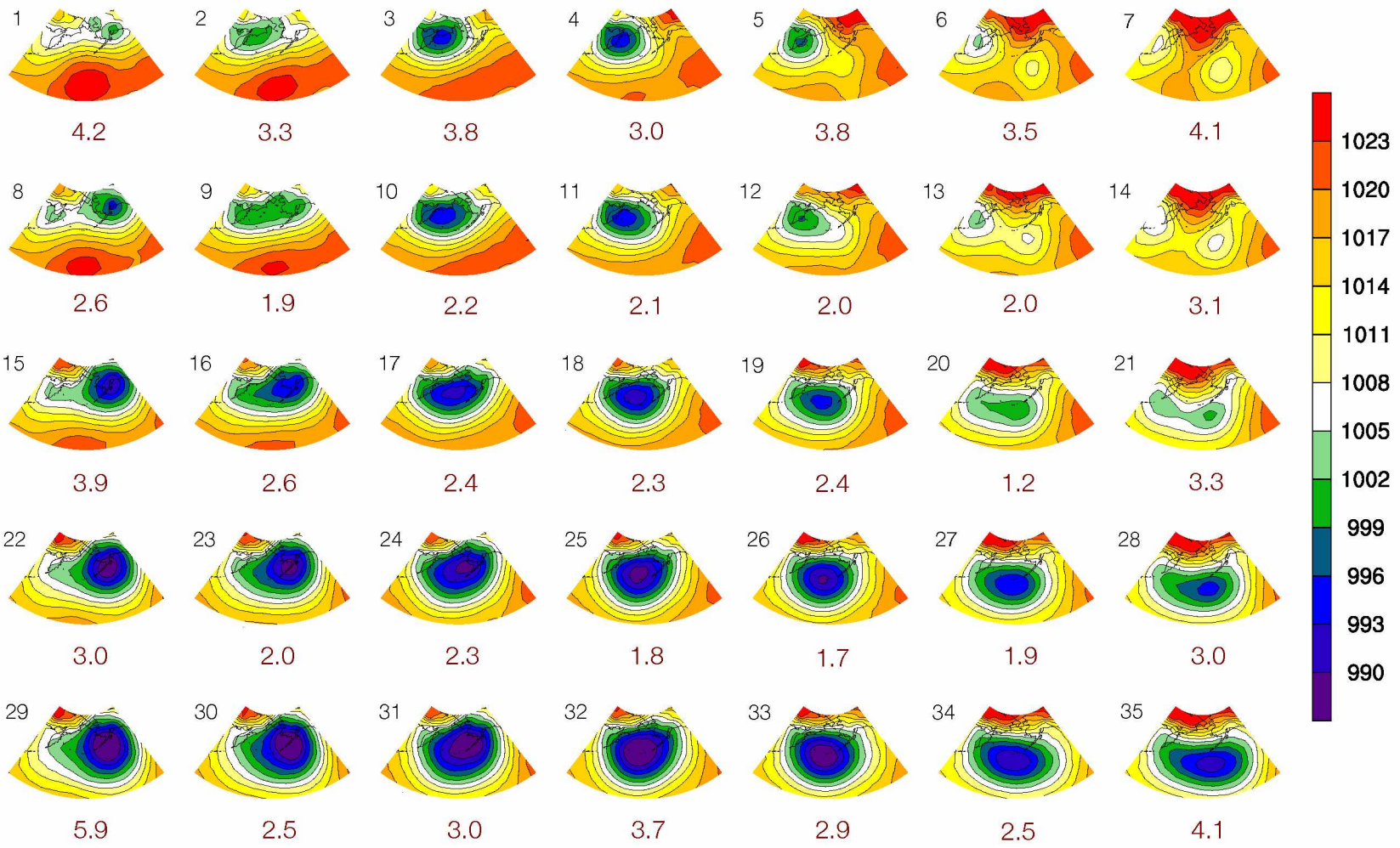

Figure 3.18 SOM space produced using daily SLP (in hPa) observations from NCEP Reanalysis for winter years with a positive NPM (see Table 2.1). Number under each map refers to the percent of total daily SLP observations matched to the map (percent occurrence).

When the correlation between the patterns favored by the positive NPM and each map in the positive NPM SOM space is computed, the three favorable patterns represent 65% of the patterns in the positive NPM SOM space. The same analysis shows that the five negative NPM favored patterns represent 48.7% of the negative NPM SOM space. When the same analysis is performed by comparing patterns favored by El Niño (using Niño4) to the maps in the positive NPM SOM space, the results show that the El Niño patterns represent 66% (64% if Niño3.4 is used) of the patterns in the positive NPM SOM space. The same analysis using La Niña and the negative NPM SOM space shows that the La Niña (using Niño4) patterns represent 54% (54% using Niño3.4) of the negative NPM SOM space.

Some ENSO representation in the NPM SOM space is likely related to the coincidence of ENSO years and NPM years. Two out of the twelve positive NPM years are also El Niño years, and nine out of the fourteen negative NPM years are also La Niña years. Such representation of ENSO within the positive and negative NPM SOM spaces supports the recent studies that indicate that the NPM is linked to tropical SST forcing (Seager et al. 2015; Hartmann 2015). However, both of these studies specifically link the NPM to the western tropics. The signals from the western (Niño4) and eastern (Niño3.4) tropical SST have almost equal presence in the NPM SOM spaces in this study (not shown), lending no definitive support to a stronger link with the western tropical Pacific.

3.2 – Summer

The climatology of summertime SLP in the North Pacific can be characterized by generally low pressure over the northern half of the domain and Alaska, and a strong subtropical high, seen in the long term climatological SLP plot in Figure 3.19.

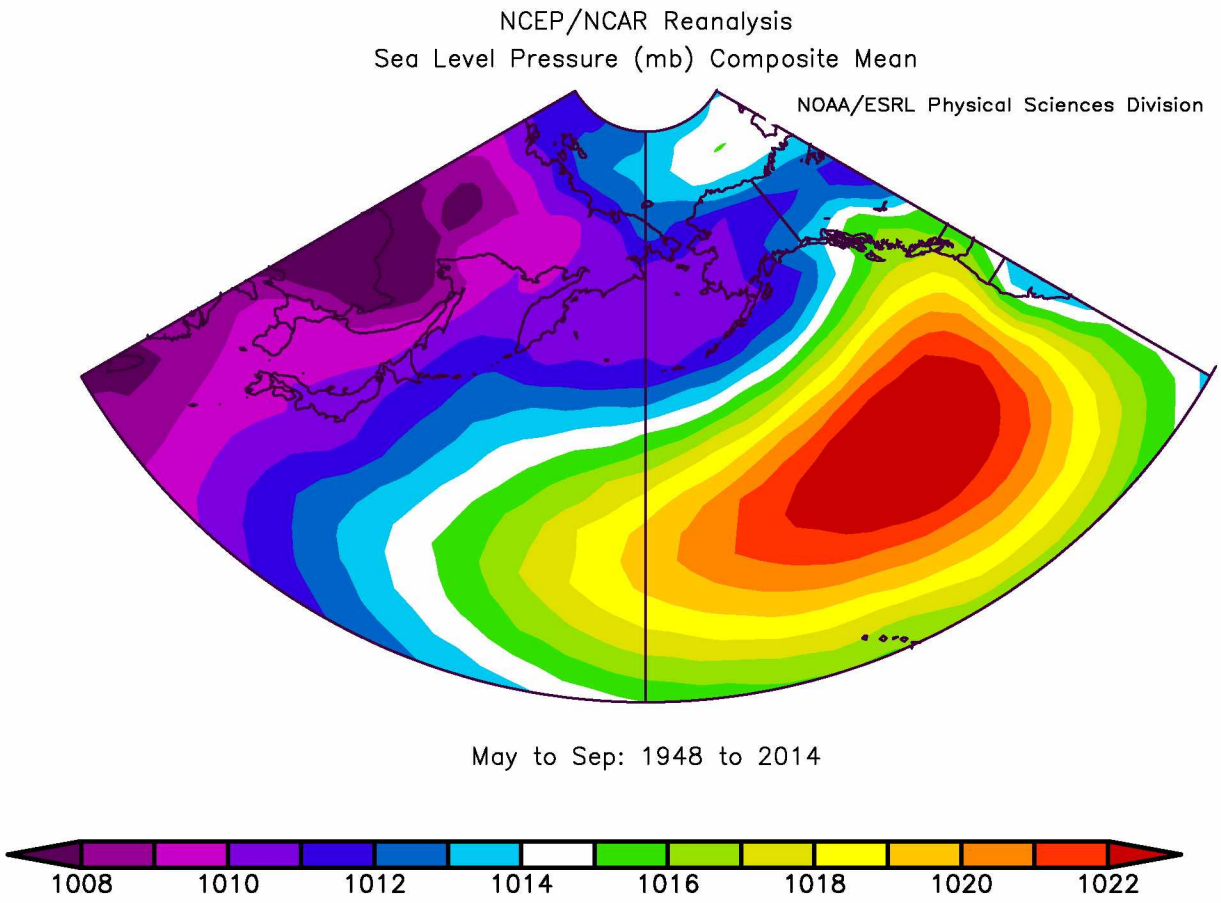

Figure 3.19 Climatological sea level pressure in hPa for summer (May-Sep) 1948-2014. Data for this plot are from NOAA/ESRL, Boulder, CO, at http://www.esrl.noaa.gov/psd/; retrieved July 2015.

In contrast to the wintertime, where a strengthened Aleutian Low was the distinctive feature, the summertime's most distinctive feature is the subtropical high. This is evident in the SOM space constructed using daily SLP patterns of all summer days between the months of May and September from 1948-2014 (Figure 3.20). This study finds that more than half of patterns represented in this SOM space are patterns whose most distinguishing feature is the subtropical high, but 100% of the patterns show at least some presence of the subtropical high. Low-pressure patterns represent 47% of the observed summertime patterns. About half of the patterns display a low over the Bering Sea while others contain a thermal low over Alaska.

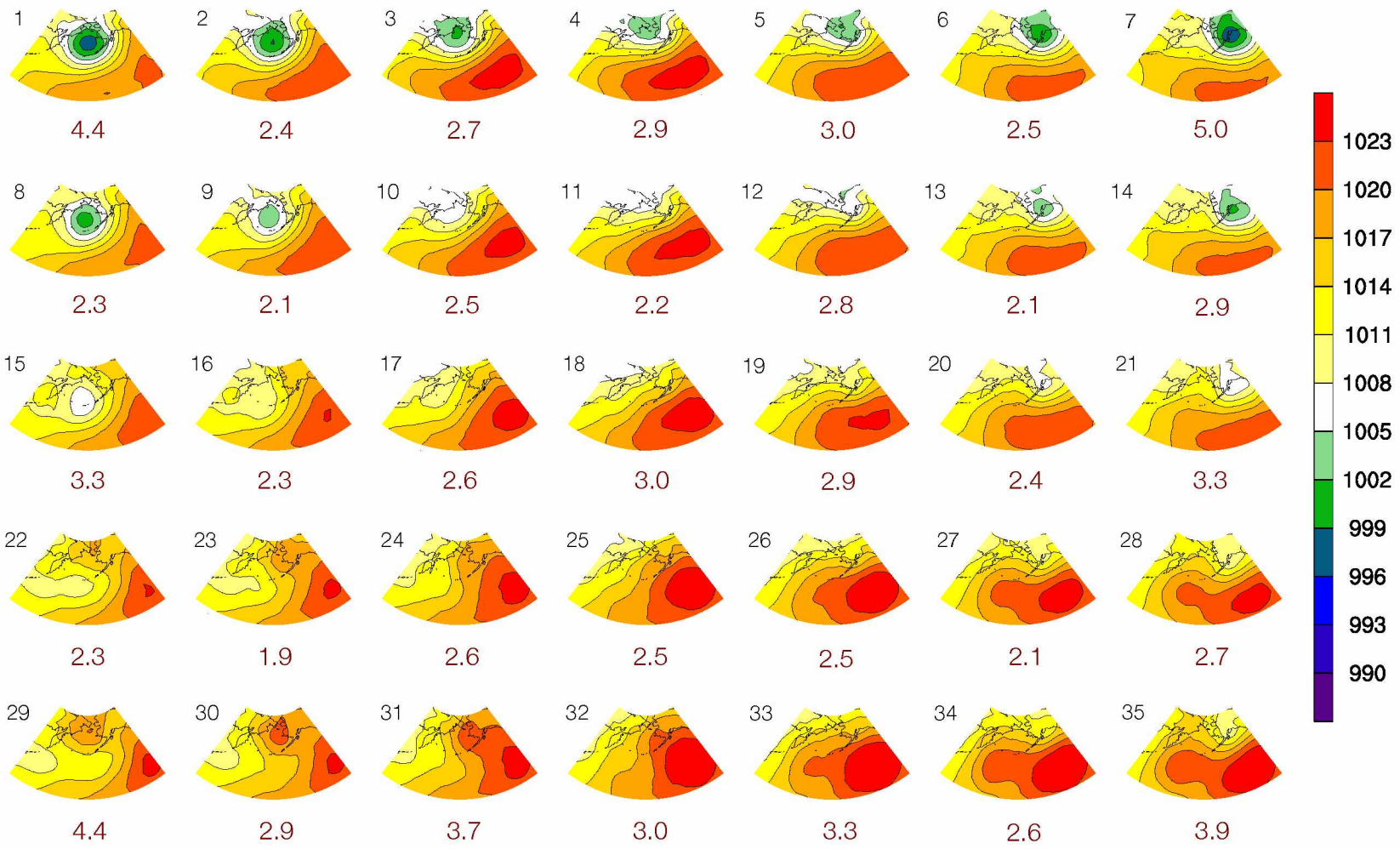

Figure 3.20 SOM space produced using daily SLP (in hPa) observations from NCEP Reanalysis for summer (May-Sep) 1948-2014. Number under each map refers to the percent of total daily SLP observations matched to the map (percent occurrence).

The differences between maps based on opposite phases of climate indices are much more subtle during the summer than during the winter, especially based on visual inspection. Indices like the PDO have essentially no signal during the summertime, and the generally weaker variability in the summer complicates some of the comparisons done between opposing phases of the indices that do show some signal.

3.2.1 – North Pacific Mode

The 1000 hPa air temperature composite anomalies over Alaska during positive and negative NPM summers show some differences (Figure 3.21 c-d). During positive NPM years, there is very little presence of any 1000 hPa temperature anomalies, while negative NPM years show a cold anomaly on the west coast of Alaska, and a warm anomaly over interior Alaska. However, while the SLP composite anomalies show some differences between positive and negative NPM years, they certainly do not show the distinct polarity present between the positive and negative NPM during winter months (Figure 3.21 a-b). Both positive and negative NPM years show lower than normal SLP over Alaska and Russia. One area where SLP anomalies are of opposite sign is south of the Aleutian Islands, where there is anomalous high pressure during positive NPM years, and weak anomalous low pressure during negative NPM years. Though there is a ridge present over the west coast of the US during the positive NPM years, it is well south of what is expected given the formal positive NPM definition.

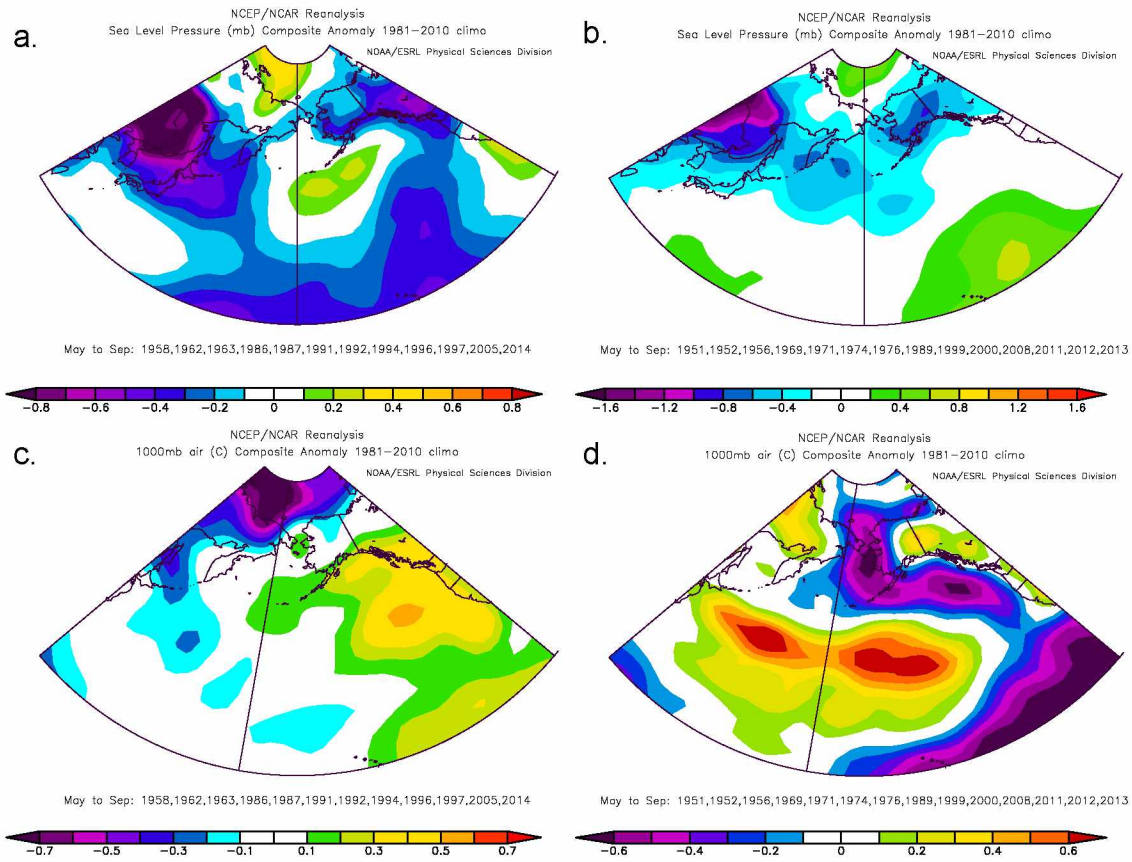

Figure 3.21 a) Sea level pressure composite anomaly for summer years with a positive NPM (see Table 2.1). b) Sea level pressure composite anomaly for summer years with a negative NPM. c) Surface air temperature composite anomaly for summer years with a positive NPM. d) Surface air temperature composite anomaly for summer years with a negative NPM. SLP is in units of hPa and temperature in °C. Data for this plot are from NOAA/ESRL, Boulder, CO, at http://www.esrl.noaa.gov/psd/; retrieved July 2015.

Favorable patterns for the positive and negative NPM years are defined similar to how they were in the winter analysis, and yields seven maps that are favored by the positive NPM (Figure 3.22), and five for the negative NPM (Figure 3.23). Though all seven positive NPM favored maps have a moderate-to-strong presence of the subtropical high, three out of the seven maps are also characterized by low pressure. Two of them include lows over the Bering Sea, while the third displays a low over coastal Alaska. All three maps would result in weak southerly flow into Alaska. The four maps without lows are all dominated by the subtropical high, resulting in weak west-southwesterly flow into Alaska. All five of the negative NPM favored maps are also heavily influenced by the subtropical high. Two out of the five also have low pressure centered over coastal

Alaska, resulting in southerly flow. The remaining three maps are only characterized by the subtropical high, and would result in generally weak westerly flow. The results are mixed when the favored maps are compared to the SOM spaces created using only daily SLP from summer years categorized as positive and negative NPM. The seven positive NPM favored maps represent 91% of the observed patterns that make up the positive NPM SOM space (Figure 3.24), and the five negative NPM favored maps represent 45% of the observed patterns in the negative NPM SOM space (Figure 3.25). However, the seven positive NPM favored maps also represent 92% of the patterns in the negative NPM SOM space, while the five negative NPM favored maps represent 48% of the positive NPM SOM space. This implies that, while there are differences in Alaska summer SAT between positive and negative NPM years, there is no evidence that they are they are related to synoptic patterns resulting from a positive/negative NPM signal. Instead, these differences are more likely related to some other large-scale features, or some local phenomena.

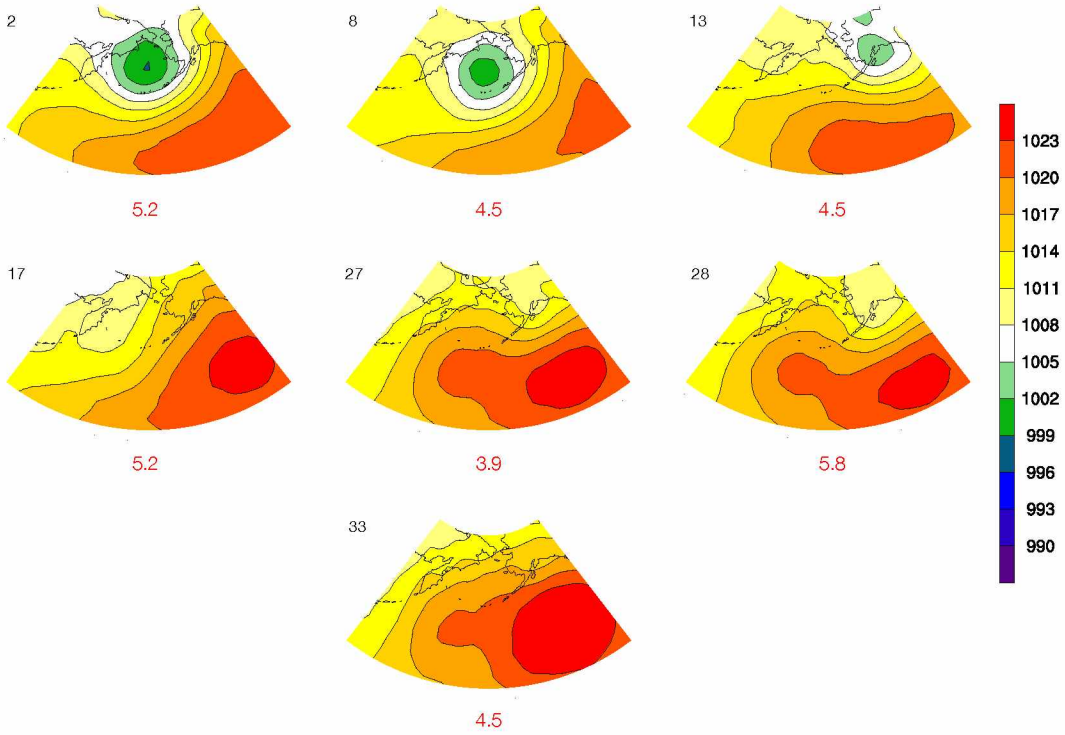

Figure 3.22 Maps from all-summer SOM space (see Figure 3.22) that are most favored by years with a positive NPM. Map displays SLP in units of hPa.

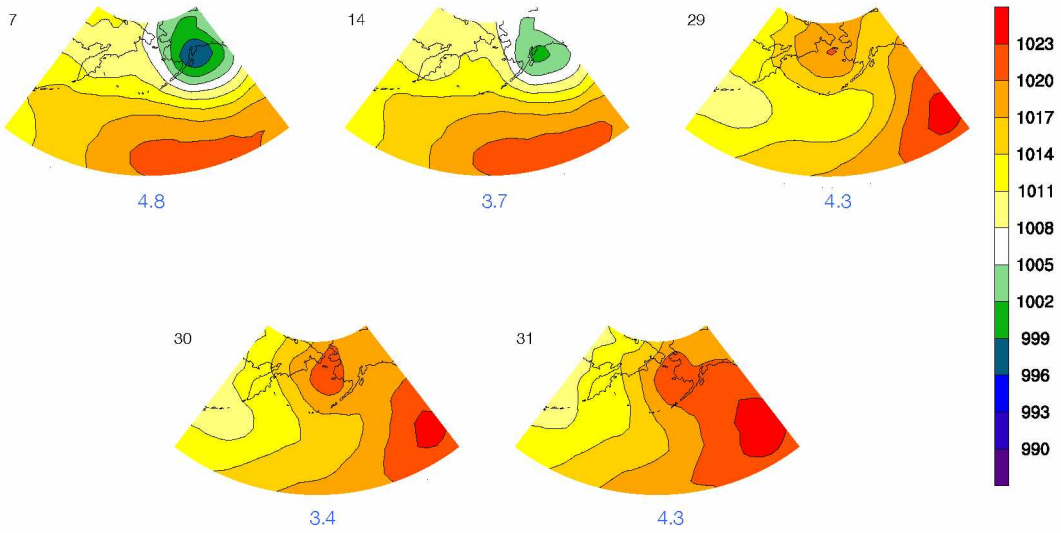

Figure 3.23 Maps from all-summer SOM space (see Figure 3.22) that are most favored by years with a negative NPM. Map displays SLP in units of hPa.

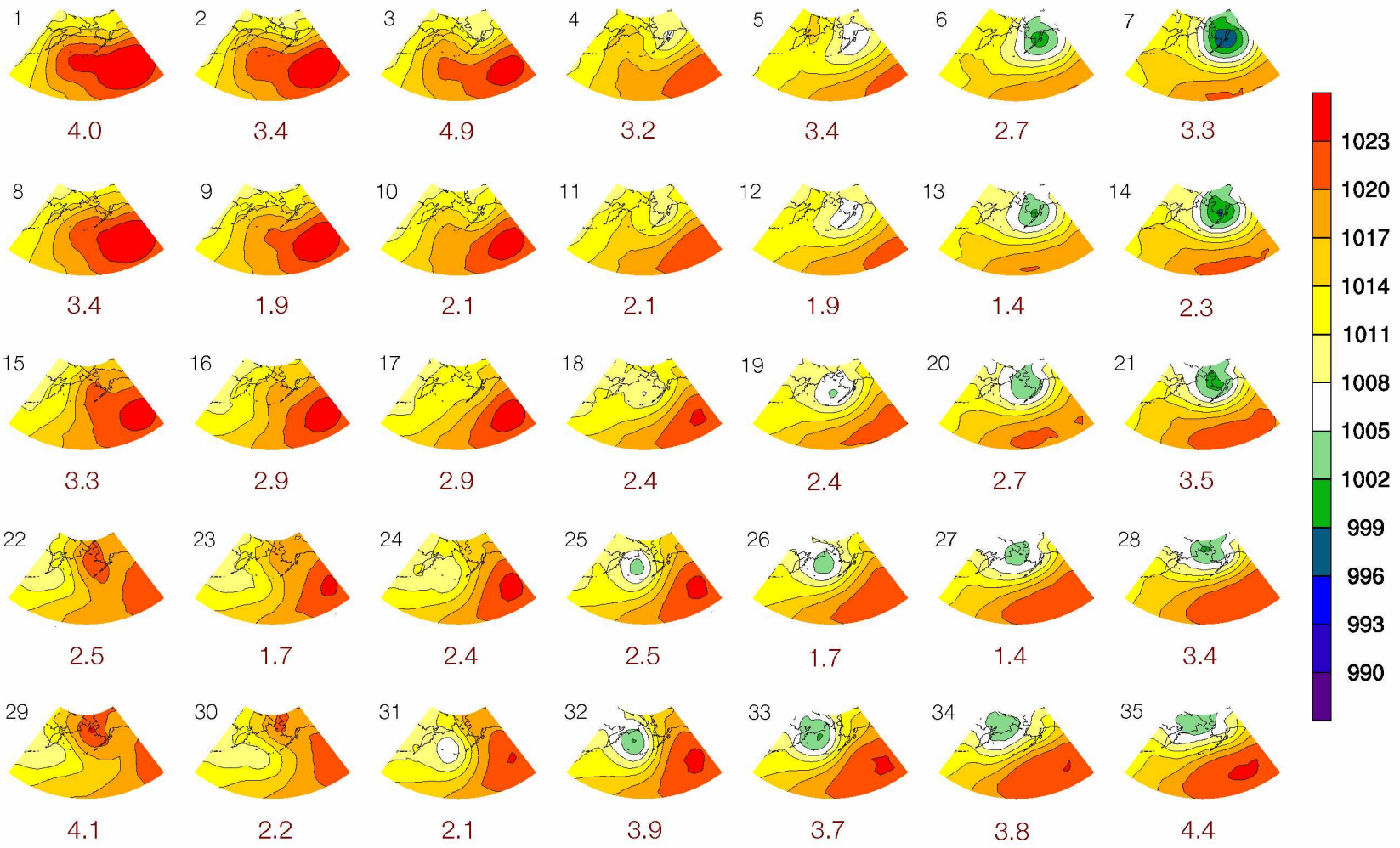

Figure 3.24 SOM space produced using daily SLP (in hPa) observations from NCEP Reanalysis for summer years with a positive NPM (see Table 2.1). Number under each map refers to the percent of total daily SLP observations matched to the map (percent occurrence).

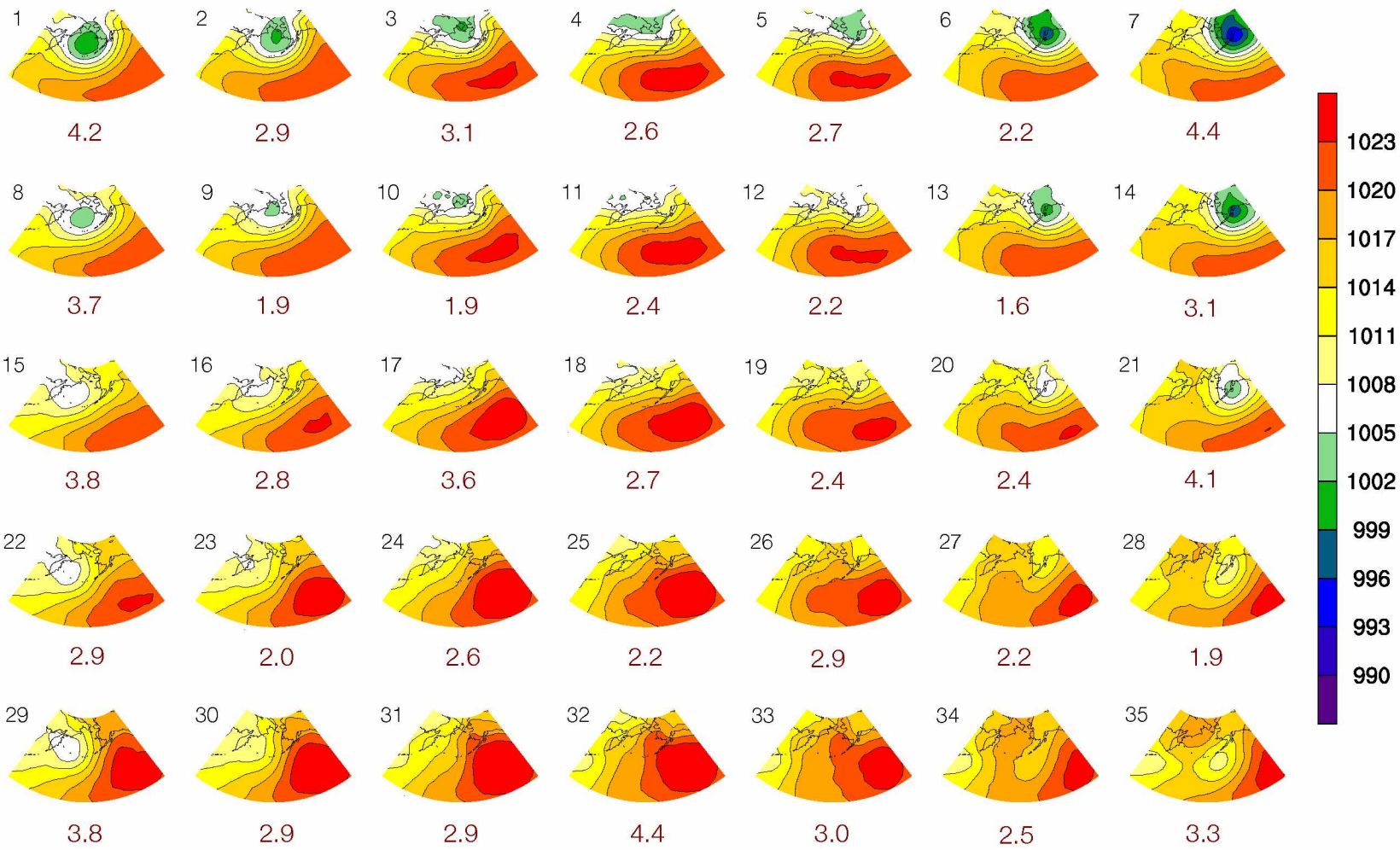

Figure 3.25 SOM space produced using daily SLP (in hPa) observations from NCEP Reanalysis for summer years with a negative NPM (see Table 2.1). Number under each map refers to the percent of total daily SLP observations matched to the map (percent occurrence).

3.2.2 – Big and small fire years in Alaska

In this study, "big fire" years refer to the ten years with the most acreage burned, while "small fire" years refer to the ten years with the least acreage burned. The climatology for big and small fire years established using the SLP composite anomaly maps displays more structure than the same maps for the positive and negative NPM (Figure 3.26). There is a notable difference in favored synoptic patterns between big and small fire years. During big fire years (for months May – September), there is a low SLP anomaly in the southwestern Gulf of Alaska, and generally southerly flow into Alaska, while there is a high SLP anomaly in the same location during small fire years.

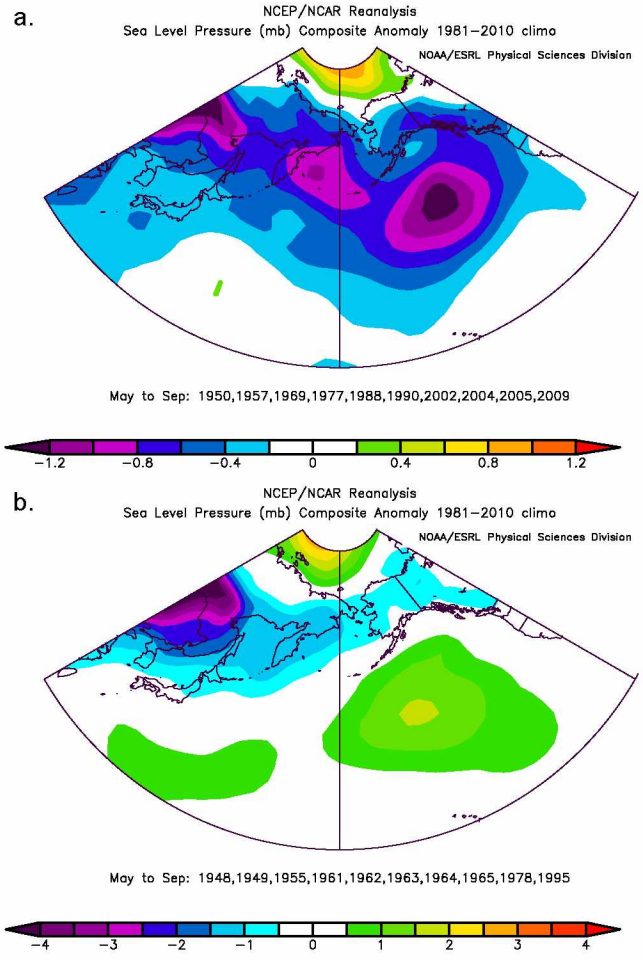

Figure 3.26 a) Sea level pressure (hPa) composite anomaly for the biggest 10 (acreage burned) summer fire years (see Table 2.1) where summer refers to May – September b) Sea level pressure (hPa) composite anomaly for the smallest 10 summer fire years. Data for this plot are from NOAA/ESRL, Boulder, CO, at http://www.esrl.noaa.gov/psd/; Retrieved July 2015.

The synoptic maps reflect this polarity in patterns. While all of the favored maps for both phases are still heavily influenced by the subtropical high, six out of the seven maps favored by big fire years prominently feature a low, with generally southerly flow over Alaska (Figure 3.27). Five out of the six maps favored by small fire years only feature high pressure, with generally western flow over Alaska (Figure 3.28).

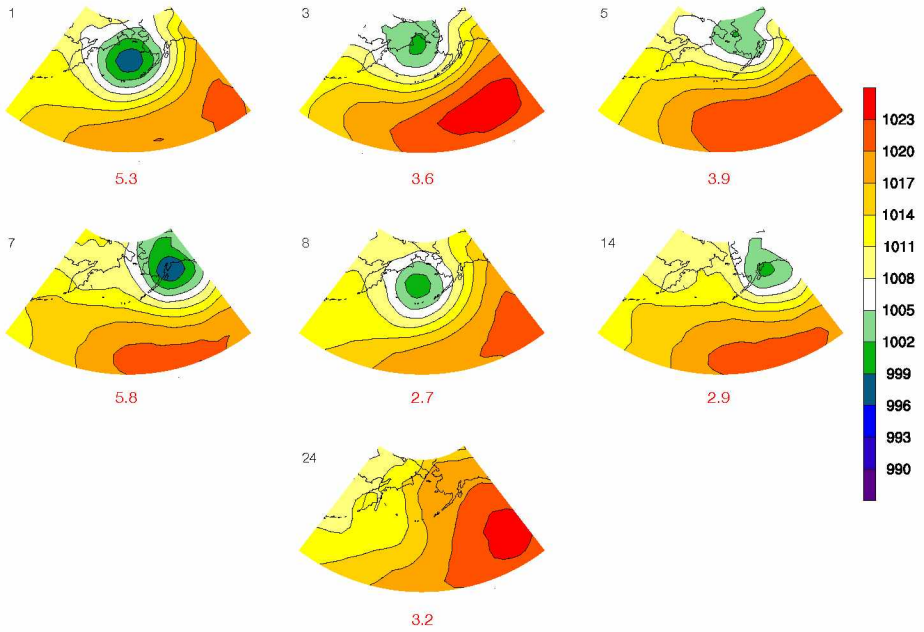

Figure 3.27 Maps from all-summer SOM space (see Figure 3.22) that are most favored by the 10 years with the biggest fires (acreage burned). Map displays SLP in units of hPa.

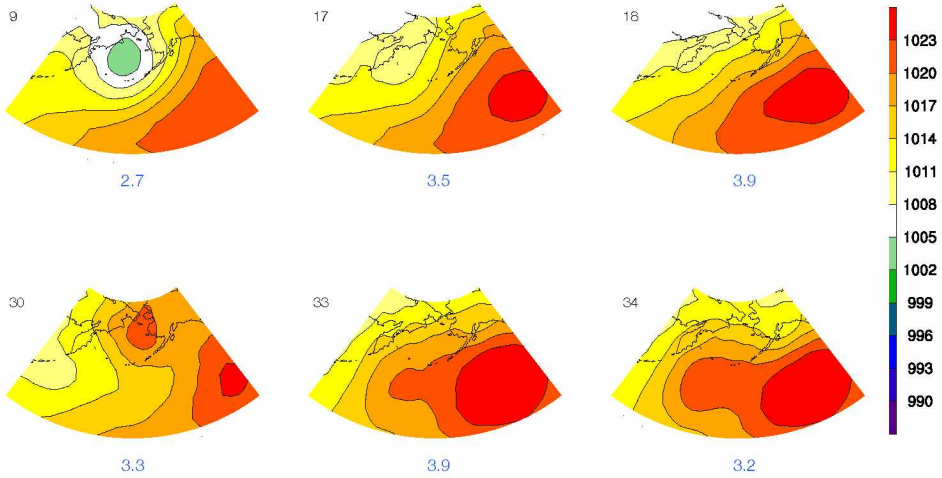

Figure 3.28 Maps from all-summer SOM space (see Figure 3.20) that are most favored by the 10 years with the smallest fires (acreage burned). Map displays SLP in units of hPa.

There does appear to be a notable difference between the synoptic patterns during big and small fire years. A scatterplot between summertime SST anomalies in the NPM region of the North Pacific and acres burned in Alaska shows that six out of seven of the biggest fire years occurred with warm anomalies in the NPM region (Figure 2.1). This coincidence suggests the possibility that the positive NPM is related to fire weather in Alaska for the extreme cases only. However, no immediate evidence of this relationship is seen in the synoptic maps for positive and negative NPM. This is perhaps an artifact of the much more subtle variations in synoptic patterns during the summer. The distribution of synoptic patterns does seem to suggest conditions that are favorable for fire generation. The dominant ridge over Canada and eastern Alaska in most of the summer patterns favors warm and dry conditions, while the Bering lows present in other patterns could fuel thunderstorm activity that produce fire-starting lightning strikes, if given enough moisture and a triggering shortwave. Further, patterns that result in a pressure gradient with higher pressure in the east, and lower pressure in the west could fuel Chinook winds into the Alaskan interior, exacerbating dry conditions. These pieces of evidence together are compelling, and suggest potential for further research into details like the frequency of transition between each SOM to be conducted.

Section 3.3 – Concluding comments

Detailing the synoptic patterns of these climate indices using the SOMs highlights variation that affects predictability. The difference in the impact for Alaska seasonal climate between PDO phases may not be as extreme as originally thought, and some within-phase variability may be expected due to the location of synoptic patterns. The SOM analysis supports the notion that rPDO and NPM signals are likely influenced by another large-scale forcing (e.g., ENSO, AO, sea ice). During summer, big and small fire years have a noticeable difference in SOM patterns, though no robust connection to large-scale climate indices (e.g., PDO, rPDO, ENSO, NPM) is immediately evident.

Chapter 4 – Conclusions

There is a strong connection between Alaska seasonal climate, and varying climate indices of the North Pacific. Climate forecasts then, depend on a detailed and accurate representation of these connections. The past decade has seen the canonical connection to one of the most prominent indices—PDO—weaken, and has detailed the connection to a newly identified index: the Pacific Blob or the North Pacific Mode (Bond et al. 2015; Hartmann 2015). The cause of this weaker PDO connection to Alaska climate remains to be seen, but recent studies suggest both a statistical and physical component (McAfee 2014). Two studies have investigated the mechanism that produced the Pacific warm blob (positive-phase of the North Pacific Mode), and both suggest a connection to western tropical SST forcing (Seager et al. 2015; Hartmann 2015). The utility of seasonal forecasts for regions like Alaska will benefit from more precision than is available using the techniques that have so far determined the canonical descriptions of these indices. Analyzing the synoptic patterns for these indices using self-organizing maps, displays the differing conditions between phases with more detail, and enables exploration of connections between these indices and more specific events, such as seasonal wildfire forecasting.

Self-organizing maps (SOMs) were generated to produce a detailed classification of the daily SLP patterns in the North Pacific that are present during different phases of the climate indices of interest for Alaska. A 7x5 grid of SOMs was constructed to produce 35 maps to best represent the daily SLP patterns for the 1948-2014 time period. The winters (NDJFM) and the summers (MJJAS) are separately considered for the study period. Additionally, SOMs were also constructed for select years associated with a particular phase of the climate indices PDO, ENSO, and Pacific blob. By comparing the SOMs for the full period with the subset of year, this study was able to identify favored SLP patterns associated with different phases of a given climate index. This identifies variation in those patterns that would not necessarily be visible in the methods used to create the canonical descriptions of these indices, such as seasonal means.

4.1 PDO and SOMs

The PDO is characterized by a change in polarity of the SLP anomaly field, where anomalously low SLP over the Aleutians during the positive phase is replaced by anomalously high SLP during the negative phase. Because the canonical relationship with Alaska's temperatures is a positive correlation, the expected temperatures in Alaska should display a similar polarity flip, where temperatures are higher than normal during positive PDO years, and lower than normal during negative years. This has not consistently been the case in recent years and the correlation with 2-m temperature has decreased (e.g., Bourne et al. 2010), when observed temperatures in Alaska have been of opposite sign to what is expected based on the phase of PDO. The synoptic patterns represented by the SOMs suggest that the weakening of the PDO-Alaska climate relationship may be due to a less stark contrast between the positive and negative phases than the canonical patterns portray, and the variable location of synoptic patterns that are otherwise similar to the canonical patterns. Since the synoptic patterns ultimately determine the weather that characterizes Alaska climate, subtleties in the way they change between the phases of PDO may result in significant differences in the resulting climate.

Patterns with moderate-to-strong low pressure in the general vicinity of the Aleutian Islands represent about 89% of the total daily patterns during positive PDO years. During negative PDO years, moderate-to-strong low patterns represent approximately 60% of the total daily patterns. This is slightly lower than the 65% of total daily patterns that are represented by the low-pressure maps when all winter years are considered, which is what produces the polarity in the SLP anomalies, but the majority of patterns during the negative PDO years are still represented by low pressure over the Aleutians. The positive phase of the PDO heavily favors low-pressure systems, but the negative phase of PDO does not—in contrast—favor high-pressure systems. Instead, the negative PDO phase favors low-pressure systems slightly less often.

Further, there is a great deal of variability within each phase of the geographical placement of the low pressure centers. The five patterns favored by the positive phase

are low-pressure patterns, and represent 88% of the patterns that comprise the positive PDO SOM space. Only three of the five patterns include the southerly flow that would result in the warm temperatures in Alaska, canonically associated with positive PDO. The remaining two have an easterly or southeasterly component that could result in some continental air mixing with marine air, and producing cooler conditions. The six maps favored by the negative phase represent 79% of the patterns establishing the negative PDO SOM space. All are characterized by high pressure to some degree, but three of the six would result in southerly or southeasterly flow into Alaska. This introduces the possibility of warmer marine air being mixed with the continental air drawn into Alaska, and would also result in warmer conditions than expected.

There are then likely to be positive PDO years that produce many strong Pacific lows that result in easterly or southeasterly flow, and cooler than expected temperatures. Similarly, there are likely to be negative PDO years containing some strong Pacific lows, with southerly flow into Alaska, and some high-pressure or ridge patterns with southeasterly flow into Alaska, both producing warmer than expected temperatures.

In an effort to reduce the variability within the PDO, a new index—rPDO—is introduced by removing the ENSO signal present in PDO (Mills and Walsh 2013; McAfee 2014). Some separation from this signal is evident in the SOMs when the phase-favoring patterns are examined for the positive and negative phases of PDO, rPDO, and ENSO. Of the five positive PDO favored patterns, only one is also favored by El Niño, but is not favored by positive rPDO. A similar effect is also seen in the negative phase, where three of the six negative PDO favored maps are also favored by La Niña, but not favored by negative PDO. Still, at least two favored maps in each phase are also favored by ENSO, either suggesting their overall importance, or some remaining shared signal.

More interestingly, this study also found that the four negative rPDO favored patterns represent a higher percentage (60%) of the patterns that make up the positive rPDO SOM space than they do of the patterns making up the negative rPDO SOM space

(58%). Such a mixed result is not present when the same analysis is done in the PDO SOM space. This is likely because, when the distinct ENSO signal is removed, some of the organized signal is removed with it. Less powerful, less organized signals are then more influential, and make the rPDO signal less well-defined. It would be beneficial to explore what other signals are present in rPDO, be they internal variability, local physical processes, or influence from other climate indices (e.g., Arctic Oscillation).

4.2 The NPM, ENSO, and SOMs

The anomalously warm SST that characterizes the positive phase of the NPM is a consequence of anomalous high SLP in the eastern North Pacific (Bond et al. 2015). Therefore, it is expected that any wintertime positive NPM favored patterns to prominently feature a high SLP in the eastern North Pacific. In fact, only one of the three positive NPM favored patterns included that feature. However, the two positive NPM favored patterns that did not include that anomalous high SLP are also patterns favored by El Niño. Additionally, an analysis using pattern correlation shows that El Niño favored patterns represent 66% of the patterns that determine the positive NPM SOM space, and La Niña favored patterns represent 54% of the patterns in the negative NPM SOM space. This indicates some influence from tropical SST forcing, which is consistent with Seager et al. (2015) and Hartmann (2015). This suggests that anomalously warm SSTs in the western tropical Pacific created a wave train that produced the persistent anomalous high SLP in the eastern North Pacific responsible for the positive NPM. However, this analysis was first done with El Niño and La Niña years defined using SST anomalies in the western tropical Niño4 box. When the analysis is replicated using El Niño and La Niña years defined using SST anomalies in the eastern Niño3.4 box, there is only a 2% decrease in El Niño representation, and no change at all in La Niña representation. So, while the synoptic patterns do support a connection to tropical SST forcing, they do not give any guidance as to whether the connection is to the western or eastern tropical Pacific.

The signature of the NPM is not as clear in the summer as it is in the winter. This is in large part due to a more quiescent synoptic environment overall. The polarity that is present in the wintertime blob anomalies is not present in the summertime anomalies, and while there are differences in SLP patterns and resulting SAT in Alaska, there is no immediate evidence—as there was in the winter—that they are connected to the synoptic patterns produced by the phases of the NPM.

For the two phases of the NPM, the synoptic patterns during the summer are so similar that the maps favored by each phase represent roughly equal, but generally more of the opposite phase's SOM space than they do of their own phase. The seven maps favored by the positive NPM represent 91% of the positive NPM SOM space, but 92% of the negative NPM SOM space. The five maps favored by the negative NPM represent 45% of the negative NPM SOM space, but 48% of the positive NPM SOM space. Even the distinct synoptic maps that make up the SOM space are too similar, or closely related to visually establish any exploitable difference between the summertime positive and negative NPM. If such a difference does exist it will likely be necessary to use a finer, or more subtle analysis to find it.

4.3 Alaska wildland fire and SOMs

The difference between big and small fire years in Alaska is much more striking than the summertime NPM phases, and suggests predictability. In this case there is a polarity flip in the SLP composite anomaly maps, where a low-pressure anomaly in the Gulf of Alaska during big fire years is replaced by a high-pressure anomaly during small fire years. The synoptic patterns are consistent with this polarity flip, as six out of seven maps favored by big fire years are distinguished by a low-pressure system, while five out of six of the maps favored by small fire years are dominated entirely by high pressure.

While differences in SLP patterns suggest seasonal predictability for synoptic patterns connected to fire weather, the conditions favoring big fires in Alaska are decided also by

the timing and evolution of these patterns, as well as their potential to produce lightning strikes. Additionally, despite initial hopes that a link between the NPM and fire weather might be found given their apparent coincidence, no immediate evidence from this study supports such a link. This is consistent with the findings of Kasischke et al. (2010) that show mixed results when using climate indices to forecast fire weather. Further analysis will be necessary to take advantage of any predictability present in the synoptic patterns associated with fire weather.

4.4 Final comments

Potential for forecasting is certainly present in the synoptic patterns presented here. Both the PDO and the NPM show a reasonable connection between the synoptic patterns produced within each phase, and the resulting variations in Alaska weather and climate. Also, the contrast between big and small fire years in the summer SOM spaces is distinct enough that forecasts may be able to take advantage of the synoptic differences. The most useful next step for all indices is likely to be an analysis of how each pattern evolves. Such an analysis exploits the continuity of the SOMs, and produces a distribution of the patterns that follow any given map after a time step. This could help forecast if a positive PDO year is likely to have many patterns resulting in southeasterly flow, and cooler than expected temperatures. Or this could help forecast if a string of high pressure patterns are followed closely by a low pressure pattern likely to produce a thunderstorm in the summer, setting up favorable conditions for wildfires in Alaska.

In order to determine the existence of predictability for indices that are less clear, like the rPDO or summertime NPM, grouping the SOMs using pattern correlation could amplify the influence of more subtle features, allowing them to be identified. Additionally, comparing them to other existing indices or climate phenomena, like the Arctic Oscillation, sea ice extent, or compositing opposite season indices may be useful for the more mixed signals, or even more clear signals, like fire years.

References

Barnston, A. G., and Y. He, 1996: Skill of canonical correlation analysis forecasts of 3-month mean surface climate in Hawaii and Alaska. *J. Climate*, **9**, 2580-2605.

Bieniek, P. A., U. S. Bhatt, L. A. Rundquist, S. D. Lindsey, X. Zhang, and R. L. Thoman,, 2011: Large-scale climate controls of Interior Alaska river ice breakup. *J. Climate*, **24**, 286-297.

Bieniek, P. A., U. S. Bhatt, R. L. Thoman, H. Angeloff, J. Partain, J. Papineau, F. Fritsch, E. Holloway, J. E. Walsh, C. Daly, M. Shulski, G. Hufford, D. F. Hill, S. Calos, and R. Gens, 2012: Climate divisions for Alaska based on objective methods. *J. Appl. Meteor. Climatol.*, **51**, 1276-1289.

Bond, N. A., and D. E. Harrison, 2006: ENSO's effect on Alaska during opposite phases of the Arctic Oscillation. *Int. J. Climatol*, **26**, 1821–1841, doi:10.1002/joc.1339.

Bond, N. A., M. F. Cronin, H. Freeland, and N. Mantua, 2015: Causes and impacts of the 2014 warm anomaly in the NE Pacific. *Geophys. Res. Lett.*, **42**, 3414-3420, doi:10.1002/2015GL063306.

Bourne, S. M., U. S. Bhatt, J. Zhang, and R. Thoman, 2010: Surface-based temperature inversions in Alaska from a climate perspective. *Atmos. Res.*, **95**, 353-366.

Cassano, E. N., and J. J. Cassano, 2009: Synoptic forcing of precipitation in the Mackenzie and Yukon River Basins. *Int. J. Climatol*, **30**, 658-674, doi:10.1002/joc.1926

Hartmann, D. L., 2015: Pacific sea surface temperature and the winter of 2014. *Geophys. Res. Lett.*, **42**, 1894-1902, doi:10.1002/2015GL063083.

Hess, J. C., C. A. Scott, G. L. Hufford, and M. D. Fleming, 2001: El Niño and its impact on fire weather conditions in Alaska. *Int. J. Wildland Fire*, **10**, 1-13.

Hewitson, B. C., and R. G. Crane, 2002: Self-organizing maps: applications to synoptic climatology. *Climate Res.*, **22**, 13-26.

Kasischke, E. S., and Coauthors, 2010: Alaska's changing fire regime – implications for the vulnerability of its boreal forests. *Can. J. Forest Res.*, **40**, 1313-1324, doi:10.1139/X10-098.

Kistler, R., and Coauthors, 2001: The NCEP-NCAR 50-year reanalysis: Monthly means CD-ROM and documentation. *Bull. Amer. Meteor. Soc.*, **82**, 247–268.

Kohonen, T., 1990: The Self-Organizing Map. *Proceedings of the IEEE*, **78**, 1464-1480.

Mantua, N. J., S. R. Hare, Y. Zhang, J. M. Wallace, and R. C. Francis, 1997: Pacific interdecadal climate oscillation with impacts on salmon production. *Bull. Amer. Meteor. Soc.*, **78**, 1069-1079.

Mantua, N. J., 2000: Pacific Decadal Oscillation (PDO). Accessed July 2015. [Available online at http://research.jisao.washington.edu/pdo/.]

McAfee, S. A., 2014: Consistency and the lack thereof in Pacific Decadal Oscillation impacts on North American winter climate. *J. Climate*, **27**, 7410-7431.

Mills, C. M., and J. E. Walsh, 2013: Seasonal Variation and Spatial Patterns of the Atmospheric Component of the Pacific Decadal Oscillation. *J. Climate,* **26**, 1575-1594, doi:10.1175/JCLI-D-12-00264.1.

Mills, C. M., and J. E. Walsh, 2014: Synoptic Activity Associated with Sea Ice Variability in the Arctic. *J. Geophys. Res. Atmos.,* **119**, 12117-12131, doi:10.1002/2014JD021604.

National Climatic Data Center, 2015: Climate at a glance. Accessed July 2015. [Available online at http://www.ncdc.noaa.gov/cag.]

National Weather Service, 2015: Observed weather stations. Accessed July 2015 [Available online at http://www.nws.noaa.gov/tg/siteloc.php.]

Newman, M., G. P. Compo, and M. A. Alexander, 2003: ENSO-forced variability of the Pacific Decadal Oscillation. *J. Climate*, **16**, 3853-3857.

Papineau, J. M., 2001: Wintertime Temperature Anomalies in Alaska Correlated with ENSO and PDO. *Int. J. Climatol.,* **21**, 1577-1592, doi:10.1002/joc.686.

Seager, R., M. Hoerling, S. Schubert, H. Wang, B. Lyon, A. Kumar, J. Nakamura, and N. Henderson, 2015: Causes and predictability of the 2011-2014 California drought. NOAA Drought Task Force Assessment Report. 42 pp.

Shulski, M., and G. Wendler, 2007: *Climate of Alaska*. University of Alaska Press, 216 pp.

Smith, C.A., and P. Sardeshmukh, 2000: The Effect of ENSO on the Intraseasonal Variance of Surface Temperature in Winter. *Int. J. Climatol*, **20**, 1543-1557.

Thompson, D.W.J., and J.M. Wallace, 1998: The Arctic Oscillation signature in the wintertime geopotential height and temperature fields. *Geophys. Res. Lett.*, **25**, 1297-1300.

Trenberth, K.E., 1990: Recent Observed Interdecadal Climate Changes in the Northern Hemisphere. *Bull. Amer. Meteor. Soc.*, **71**, 988-993.

Xue, Y., T. M. Smith, and R. W. Reynolds, 2003: Interdecadal changes of 30-yr SST normals during 1871-2000. *J.Climate*, **16**, 1601-1612.